Namdar
Protection and Control of Modern Power Systems (2022) 7:48
https://doi.org/10.1186/s41601-022-00269-4

Protection and Control of Modern Power Systems

ORIGINAL RESEARCH

Open Access

A robust principal component analysis-based approach for detection of a stator inter-turn fault in induction motors

Ali Namdar*

Abstract

Health condition monitoring of induction motors is important because of their vital role and wide us in a variety of industries. A stator inter-turn fault (SITF) is considered to be the most common electrical failure according to statistical studies. In this paper, an algorithm for the detection of an SITF is presented. It is based on one of the blind source separation techniques called principal component analysis (PCA). The proposed algorithm uses PCA to discriminate between the faulty components of motor current signatures and motor voltage signatures from other components. The standard deviation of one of the decomposed vectors is used as a statistical SITF criterion. The proposed criterion is robust to non-fault conditions including voltage quality problems and large mechanical load changes as well as harmonic contaminants in the voltage supply. In addition, with a straightforward and low computational burden in the fault detection process, the proposed method is computationally efficient. To evaluate the performance of the proposed method, large numbers of practical and simulation scenarios are considered, and the results confirm the good performance, high degree of accuracy, and good convergence speed of the proposed method.

Keywords: Induction motors (IMs), Stator inter-turn fault (SITF), Voltage quality problem, Principal component analysis (PCA)

1 Introduction

Because they give good and cost-efficient performance, induction motors (IMs) are the most widely used rotating electric machines over a range of industries. However, IMs suffer from failures due to mechanical, environmental, and electrical stress [1]. Statistical reports on IM failures reveal that around 30–40% of the electrical failures can be attributed to the stator winding [2]. Typically, when a short circuit occurs between two turns of the stator winding and the voltage difference between the turns overcomes their insulation capacity, an insulation breakdown results in a stator inter-turn fault (SITF). Therefore, stator winding faults usually start with a SITF and if not detected in a timely fashion, they can move to other high-intensity faults, including coil-to-coil, phase-to-phase, or phase-to-ground faults [3].

1.1 Motivation and literature review

Recently, several methods have been presented to detect stator winding faults. These methods can be broadly categorized into model-based and signal-based techniques [4]. Although model-based methods are found on a single analytical model they are less accurate and more complex than signal-based methods [5]. In general, signal-based approaches are classified into the two categories of invasive and non-invasive methods [6]. Various tools are used for analyzing the signals such as, in the time domain correlation functions [7], in the frequency domain the Fast Fourier Transform (FFT) [8], and in the time–frequency domain the Short Time Fourier Transform (STFT) [9] and Wavelet Transform (WT) [10]. However, they all have limitations and drawbacks that require further

*Correspondence: alinamdaribiloo@gmail.com

School of Electrical and Computer Engineering, Shiraz University, Shiraz, Iran

investigation. For instance, although FFT is the most well-known signal analysis tool in the steady-state it has insufficient accuracy during dynamic conditions. Time–frequency domain analysis can be used to overcome the weaknesses of FFT, though unfortunately, the biggest drawback of STFT is the use of a fixed-size window for analyzing all frequencies. To overcome the shortcomings of STFT-based algorithms, WT and principal component analysis (PCA)-based algorithms can be adopted. These decompose the input signals into several components for better resolution while retaining important components in the original signals. In WT, these components are called approximations and details, whereas in PCA they are called principal components (PC). Although the use of a variable size-window in the WT can solve the shortcoming of STFT-based algorithms, it has some weaknesses compared to PCA, e.g.: (1) it needs different sampling frequencies for different frequency sub-bands; (2) it has severe reliance on the suitable choice of the mother wavelet signal (Haar, Daubechies, Symlets, …); and (3) it has dependence on the decomposition approach (DWT and WPT) and method of approximating the analytical signal (via FFT or FIR) [11]. Thus, owing to the disadvantages of WT compared to PCA, the use of a PCA-based algorithm as an appropriate and efficient technique is recommended to address the weaknesses of other techniques.

In invasive methods, sensors play an important role and are physically installed on the electrical machine to capture the required signals. Typically, the extracted signals are temperature [12], stator frame vibration [13], and acoustic noise [14]. The proposed indices based on MCS and MVS are stator current envelope [15], instantaneous total harmonic distortion (ITHD) [16], instantaneous frequency [17], air-gap torque [18], instantaneous electrical power [19], negative sequence stator current [20], and stator current zero-crossing [20]. The main advantages of non-invasive methods compared to the invasive include lower cost and less disturbance in normal operation because there is no physical installation of sensors, better performance in detection of weak faults, and higher reliability [6].

Because of the overlap between signatures related to fault and non-fault conditions, some of the indices listed for SITF detection are not reliable for non-fault conditions such as voltage quality problems [21]. As an illustrative example, ITHD and instantaneous frequency indices are not robust to non-fault conditions such as voltage sag and voltage swell problems. Furthermore, air-gap torque and negative sequence stator current may experience maloperation in an unbalanced power supply voltage.

Aside from the mentioned techniques, a variety of other methods based on artificial intelligence have been suggested for the detection of SITFs. These are categorized in Table 1. The most common approaches here are fuzzy logic, expert systems, evolutionary algorithms and artificial neural networks [6]. The main drawbacks of fuzzy logic based methods are unpromising efficiency in inaccurate inputs and complete dependence on expertise and human intelligence, whereas methods based on expert systems have less flexibility, insufficient accuracy and higher complexity. Evolutionary algorithms can be used for detection of a stator inter turn fault but often suffer from the need for considerable time so are unsuitable in online fault diagnosis [6].

Methods based on MLP and RBF algorithms, which are generally called conventional neural networks, suffer from two main shortcomings. These include the inability to self-learn without feature extraction and the need for a huge dataset for training. In modern neural network-based methods such as deep learning, the self-learning problem is solved. However they still have the main weaknesses as briefly tabulated in Table 1.

Although SVM can handle outliers better and provides promising accuracy in fault detection, it still suffers from the need for large data and has sluggish performance in large data. In k-NN, easy implementation is a prominent advantage but having slow real time performance and being sensitive to outliers are its main weaknesses. One of the main advantages of ANN is the adjustability for better classification, although its main drawback is overfitting. Merits of using decision trees and random forest include immunity against external noise, but overfitting and a long training period are their big weaknesses. Naive Bayes is another algorithm that is used because of its robustness to noise. Nonetheless, this classifier depends on the probability of two independent sets. Deep Learning is the latest approach used in research in the field of fault detection, including CNN, RNN, LSTM and AE. Although this technique provides good accuracy and is able to solve the self-learning without feature extraction problem, its biggest drawbacks are the need for a large amount of data in different conditions and also that the training process requires a long time. Thus, this technique requires a powerful processor to perform the training process on a large database. This is the most prominent weakness compared to other methods. As an overall trend, the need for massive data is considered the biggest weaknesses of artificial intelligence-based methods.

1.2 Aim and contribution

In this paper, a robust strategy for detecting a SITF based on MCS and MVS is proposed to minimize the interference with other possible transient disturbances. In general, the deviation of the post-disturbance signal from the

Table 1 The categorization of artificial intelligence-based methods

Method based				Main weaknesses
Fuzzy logic [22]				1. Necessity to large accessible data 2. Unpromising efficiency in inaccurate inputs 3. complete dependence on expertise and human intelligence
Expert systems [23]				1. Insufficient accuracy 2. Complexity 3. Low flexibility
Evolutionary algorithms [24]				1. Require long time 2. Unsuitable for online fault diagnosis
Artificial neural network [25]	Conventional neural networks	RBF [26]		1. Inability to self-learning without feature extraction 2. Necessity to large accessible data
		MLP [26]		
		SVM [27]		1. Necessity to large accessible data 2. Sluggish Performance due to large data requirement
		k-NN [28]		1. Necessity to large accessible data 2. Slow performance in real time 3. Outlier-sensitivity
		ANN [29]		1. Necessity to large accessible data 2. Overfitting
	Modern neural networks	Decision trees and random forest [30]		1. Necessity to large accessible data 2. The longest training period 2. Overfitting
		Native Bayes [31]		1. Necessity to large accessible data 2. Suitable only for independent features
		Deep learning	CNN [32]	1. large data requirement 2. Need long time for training
			RNN [33]	
			AE [34]	
			LSTM [35]	

pre-disturbance one (which has a sinusoidal waveform) is the basis of the proposed method. The main steps of the proposed method are listed as follows:

I. Once a SITF happens, some distortions appear in the ideal sinusoidal current and voltage signals. Using a recursive and straightforward formulation based on PCA,
II. those fault-related blind sources which are most present in one of the decomposed vectors are extracted.
III. The post-disturbance signals may be different from the pre-disturbance signals. In that case the fault can be identified using extracted decomposed vectors. The standard deviation of one of the decomposed vectors is proposed as a statistical criterion to detect SITFs. The criterion value exceeds the defined threshold in a fault condition, whereas in normal conditions, such as mechanical load change, it is less than the defined threshold value.
IV. An auxiliary criterion based on voltage signal is introduced to increase the robustness of the proposed criterion against non-fault voltage conditions such as sag, swell, and imbalance.
V. Low-computational mathematical burden, fast response, as well as comprehensiveness are some of the main merits of the proposed method.

1.3 Paper organization

In the rest of the paper, Sect. 2 introduces a mathematical model of IMs with STIF and fault resistance (R_f), while in Sect. 3, the theory of the PCA algorithm and an explanation of the proposed method are presented in more detail. To confirm the performance of the proposed method, a simulation study is investigated under different conditions in Sect. 4, whereas in Sect. 5, the validation of the proposed method with experimental data is provided. Section 6 discusses the impact of some important parameters on the proposed criterion and consequently experimental implementation requirements and factors affecting accuracy are investigated in Sect. 7. In Sect. 8, a comparison between the proposed method and other similar methods is carried out, and finally, conclusions are presented in Sect. 9.

2 Mathematical model of IM considering SITF

To assess the performance of fault detection algorithms and study the changes of the variables in different motor operating conditions, it is very important to use a suitable model of IM. Several IM models have been introduced for different targets [36]. Here, a qd0 model considering an SITF with fault resistance (R_f) is considered. This has been presented in [37]. In general, the following assumptions are made in this model [38]:

I. The motor air gap is considered to be uniform, and hence the notching effects and generating space harmonics are ignored.
II. Temperature-dependent parameters in the model do not change because of the assumption of constant motor temperature.
III. There is unsaturation of the magnetic field due to a constant permeability.
IV. Along the air gap, the generated magneto-motive forces of stator and rotor phases propagate sinusoidally.
V. Hysteresis, skin, and eddy current effects are not taken into account.

Figure 1 illustrates a three-phase stator winding in star connection with an SITF in phase "a" where μ is the ratio of the shorted turns to the total number of turns in one phase. Accordingly, the stator and rotor circuit equations of IM considering an SITF based on Kirchhoff's circuit theory according to the defined parameters in the Nomenclature section are written as:

$$[V_{abcs}]=[R_s][I_{abcs}]+\frac{d}{dt}\left[[L_{ss}][I_{abcs}]+[L_{sr}][I_{abcr}]-\left[L_{sf}\right]I_f\right]-[Z_a]I_f \tag{1}$$

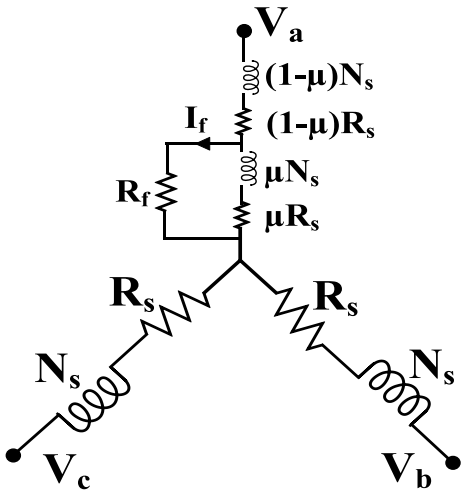

Fig. 1 Stator winding with SITF on single phase

$$0=[R_r]\left[I_{abcr}\right]+\frac{d}{dt}\left[[L_{sr}]^T[I_{abcs}]+[L_{rr}][I_{abcr}]-\left[L_{rf}\right]I_f\right] \tag{2}$$

$$0=\mu R_s I_{as}-\left(\mu R_s+R_f\right)I_f+\frac{d}{dt}\left[\left[L_{sf}\right]^T[I_{abcs}]+\left[L_{rf}\right]^T[I_{abcr}]-L_{ff}I_f\right] \tag{3}$$

where $V_{abcs}=[V_aV_bV_c]^T$, $I_{abcs}=[I_aI_bI_c]^T$, $[Z_a]=[\mu R_s 00]^T$,$[R_s]=diag[R_sR_sR_s]$ and $[R_r]=diag[R_rR_rR_r]$. It is worth noting that the suffixes of s, r and f are related to the stator, rotor, and fault, respectively.

The electromagnetic torque and rotor speed are written as:

$$T_{em}=\frac{P}{2}[I_{abcs}]^T\frac{d}{d\theta_r}[L_{sr}][I_{abcr}]-\frac{P}{2}I_f\frac{d}{d\theta_r}\left[L_{rf}\right][I_{abcr}] \tag{4}$$

$$\frac{d}{dt}\omega_r=\frac{P}{2}\frac{T_{em}-T_L}{J} \tag{5}$$

To separate the abc parameters of the motor, Eqs. (1)-(6) are transformed into the stationary reference frame with direct-quadrature-zero (qd0) transformation matrix as:

$$\frac{d}{dt}\omega_r=\frac{P}{2}\frac{T_{em}-T_L}{J} \tag{6}$$

where $\left[\lambda_{qd0s}\right]$, $\left[\lambda_{qd0s}\right]$ and $\left[\lambda_{qd0s}\right]$ are the stator fluxes, rotor fluxes and stator short-circuit flux in the qd0 reference frame, respectively, and $T[Z_a]=\left[\frac{2}{3}\mu R_s 0\frac{1}{3}\mu R_s\right]$.

The flux equations in the stationary reference frame qd0 can be expressed as:

$$\left[\lambda_{qd0s}\right]=\begin{bmatrix}L_s&0&0\\0&L_s&0\\0&0&L_{ls}\end{bmatrix}[I_{qd0s}]+\begin{bmatrix}L_m&0&0\\0&L_m&0\\0&0&0\end{bmatrix}[I_{qd0r}]-\begin{bmatrix}A_mL_{ms}+\frac{2}{3}\mu^2L_{ls}\\-B_mL_{ms}\\\frac{1}{3}\mu^2L_{ls}\end{bmatrix}I_f \tag{7}$$

$$\left[\lambda_{qd0r}\right]=\begin{bmatrix}L_r&0&0\\0&L_r&0\\0&0&L_{lr}\end{bmatrix}[I_{qd0r}]+\begin{bmatrix}L_m&0&0\\0&L_m&0\\0&0&0\end{bmatrix}[I_{qd0s}]-\begin{bmatrix}A_mL_{ms}\\-B_mL_{ms}\\0\end{bmatrix}I_f \tag{8}$$

$$\lambda_f=\frac{3}{2}\begin{bmatrix}A_mL_{ms}+\frac{2}{3}\mu^2L_{ls}\\-B_mL_{ms}\\\frac{2}{3}\mu^2L_{ls}\end{bmatrix}^T\left[I_{qd0s}\right]+\frac{3}{2}\begin{bmatrix}A_mL_{ms}\\-B_mL_{ms}\\0\end{bmatrix}^T\left[I_{qd0r}\right] \tag{9}$$

where $L_s=L_{ls}+\frac{3}{2}L_{ms}$, $L_r=L_{lr}+\frac{3}{2}L_{ms}$ and $L_m=\frac{3}{2}L_{ms}$. A_m and B_m are introduced in Tables 1 and 2 of [37] and have constant values. Thus, the electromagnetic torque equation in the stationary reference frame can be rewritten as:

$$T_{em} = \frac{3P}{4}\left[L_m\left(I_{qs}I_{dr} - I_{ds}I_{qr}\right) + L_{drf}I_{qr}I_f - L_{qrf}I_{dr}I_f\right] \tag{10}$$

where $L_{drf} = -B_m L_{ms}$ and $L_{qrf} = A_m L_{ms}$.

It should be noted that the appellation of the model variables is described in the Nomenclature section.

3 Proposed inter-turn fault detection method

From the study presented in [39], once an STIF occurs, some harmonics will be manifested in the air-gap flux density and induced in the stator current, as:

$$f_{Fault} = f_{50Hz}\left[\frac{h}{p}(1-s) \mp m\right] \tag{11}$$

where f_{Fault} and f_{50Hz} denote the SITF harmonics relevant to the order $h = 1, 2, 3, \ldots$, and fundamental frequency, respectively. p and s are the number of pole pairs and motor slips, respectively. The order of the stator time harmonics is defined by $m = 1, 3, 5, \ldots$.

Figure 2a illustrates the phase-a stator current and Fig. 2b shows the corresponding spectrogram. As seen in Fig. 2a, an SITF occurred at $t = 1s$. As shown in Fig. 2b, the B-zone power increases relative to the A-zone power because of the appearance of the SITF components according to (13) in the stator current. Hence, to study the behavior of the SITF components, it is reasonable to pass the stator current through a high-pass filter with a cut-off frequency of 150 Hz. A PCA algorithm is then employed to extract the principal components for detection of the SITF. In the following sub-sections, the theory of PCA is discussed.

3.1 Theory of PCA in detail

PCA is an orthogonal transform for feature extraction and is one of the blind source separation and dimensionality-reduction techniques that uses mathematical principles to transform a large set of possibly correlated variables into their components, namely, principal components that contain most of the required information.

Figure 3 introduces PCA to better explain the PCA theory. As illustrated, the two vectors of X_1 and X_2 are the data vectors. However, as can be seen, from either the X_1 or X_2 axis, the data cannot be classified, but it becomes sufficient if these data vectors are transferred to D_1 and D_2 by a mapping matrix. Given that the data around the D_1 axis have more variance than around the D_2 axis, so the D_1 axis has better separability than the D_2 axis.

In this analysis, the number of the measured signals and the sample number of each measured signal are denoted by M and N, respectively, and the principal

Table 2 The energy of different decomposed vectors

Scenario		$E(D_1)$	$E(D_2)$	$E(D_3)$	$E(D_4)$	$E(D_5)$	$E(D_6)$
Inter-turn fault							
$\mu = 0.02$ to $\mu = 0.4$	V	29.42	28.86	31.79	30.53	30.73	29.83
	I	63.79	54.56	94.86	71.63	24.64	54.91
$R_f = 0\ \Omega$ to $R_f = 2000\ \Omega$	V	29.73	28.52	30.85	29.43	30.02	29.84
	I	52.85	52.12	93.94	67.08	23.76	55.78
THD = 0.2% to *THD* = 10.2%	V	29.73	28.43	30.91	28.83	29.84	28.31
	I	51.76	48.97	91.43	68.52	18.92	48.63
SNR = 60 db to SNR = 30 db	V	31.44	30.05	32.33	31.47	31.45	30.92
	I	67.73	48.65	93.64	72.58	28.73	55.83
Voltage quality problems							
Voltage sag 10% to 35%	V	61.52	54.51	95.97	82.85	28.43	58.71
	I	56.42	51.12	86.51	43.04	33.94	34.95
Voltage swell 10% to 35%	V	62.84	58.43	96.81	84.43	36.79	59.46
	I	53.86	48.97	89.56	47.76	32.79	33.52
Unbalanced voltage 2% to 5%	V	60.63	52.61	94.58	81.63	34.51	58.06
	I	50.08	43.94	85.53	46.53	28.62	31.48
Capacitor switching with increase the power factor from 0.74 to 1	V	63.72	56.47	95.79	82.34	33.52	53.74
	I	52.83	46.71	86.84	44.41	31.44	32.57
Parallel motor switching	V	62.74	53.27	94.51	82.47	33.92	57.95
	I	52.63	46.97	88.47	44.15	37.82	34.57
Mechanical load 0.5 p.u to 1.8 p.u	V	11.24	12.47	12.87	10.98	11.07	11.43
	I	25.35	24.68	26.87	25.41	23.47	24.35

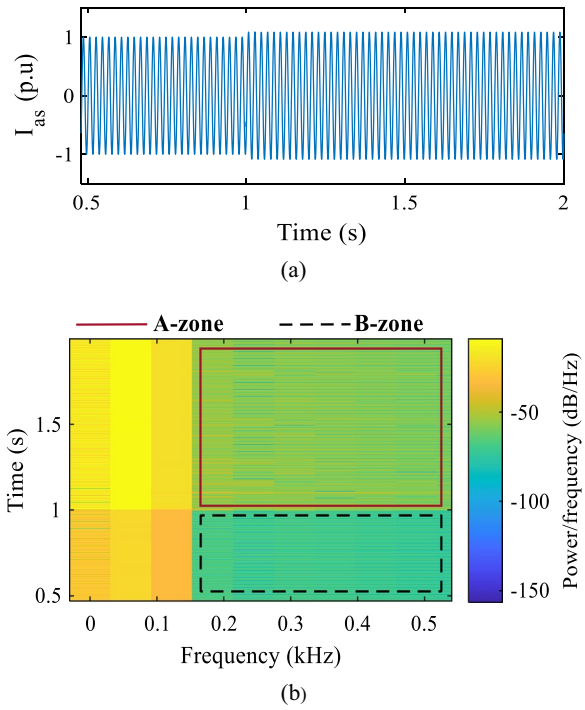

Fig. 2 A simulated inter-turn fault ($\mu = 0.05$) characteristics, **a** The a-phase stator current signal, **b** a-phase stator current spectrogram

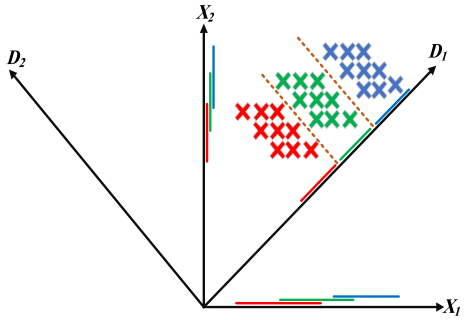

Fig. 3 Introduction of principal component analysis (PCA)

components are constructed as linear combinations of the measured signals. Hence, the decomposed vectors $D_j(j = 1, \ldots, K), K \leq M$ are shown as:

$$D_j = A_{j,1}x_1 + \ldots + A_{j,M}x_M for j = 1, \ldots, K \tag{12}$$

where $X = [x_1, x_2, \ldots, x_M]$ is the set of measured signals with dimension $N \times M$, while A represents the mapping weight matrix with dimension $M \times K$. Equation (14) can be rewritten in matrix form as:

$$D = XA \tag{13}$$

To compute A, eigenvectors of the covariance matrix are required. So, in the first step, the covariance matrix C with dimensions $M \times M$ is calculated through multiplying the measured signals by their transposes, as:

$$C = \frac{1}{N}X^T X \tag{14}$$

In the covariance matrix, the relationship between the two dimensions can have positive, negative, and zero values. Positive and negative values of covariance show directly and indirectly proportional between the two dimensions, respectively, while zero value of covariance represents that the two dimensions are independent. In the next step, the eigenvectors of the covariance matrix are obtained, as:

$$V^{-1}CV = E \tag{15}$$

where V and E are eigenvector matrices with dimensions $M \times M$ and a diagonal matrix whose diagonal elements are eigenvalues corresponding to its eigenvector, respectively. To find the mapping weight matrix, eigenvectors should be reordered according to the size of the corresponding eigenvalues in a way that the first eigenvector is proportional to the largest eigenvalue and the last eigenvector is proportional to the smallest eigenvalue. Hereafter, the first K columns of the reordered eigenvector matrix are selected as A.

3.2 Implementation of the proposed algorithm

According to PCA theory, the number of sources considered to be separated from each other is fewer than or equal to the number of measured signals ($K \leq M$). Generally, a fault may occur in one phase or another non-fault situation may affect the three-phase currents and voltages. In this way, in the proposed method, the three-phase motor signals are considered as inputs to the proposed method.

As mentioned in the previous section, a high-pass filter with a cutoff frequency of 150 Hz is used to eliminate the SITF components. Figure 4 illustrates the high-frequency components of the three-phase currents in the case of an inter-turn fault condition ($\mu = 0.05$).

As observed in Fig. 4, two consecutive data windows are used in the proposed method. Hence, X is defined as:

$$X = \left[x_{ah}^n \; x_{bh}^n \; x_{ch}^n \; x_{ah}^{n-1} \; x_{bh}^{n-1} \; x_{ch}^{n-1} \right] \tag{16}$$

where x_{ah}^n, x_{bh}^n and x_{ch}^n are the high-frequency vectors of the signals in the running window. Also, the high-frequency vectors of the signals in the previous window are denoted as x_{ah}^{n-1}, x_{bh}^{n-1} and x_{ch}^{n-1}. It should be noted that.

x can be the measured stator three-phase currents or voltages, while n is the window number.

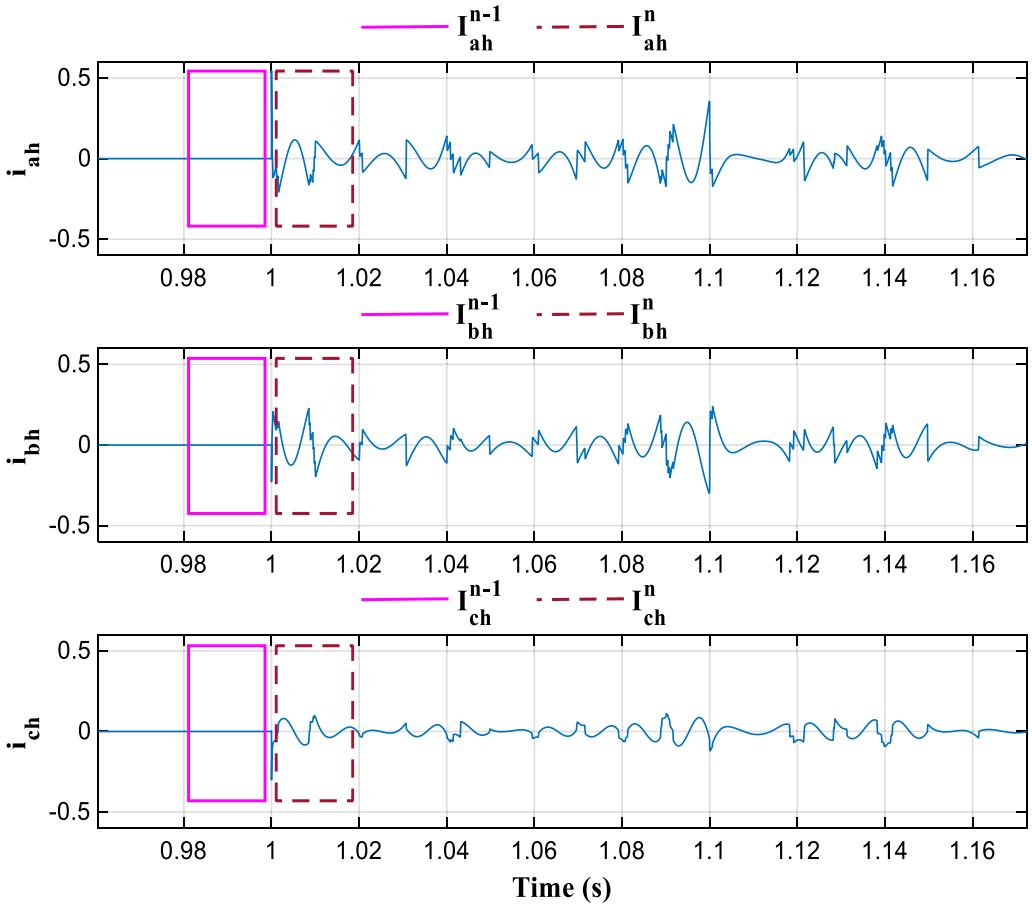

Fig. 4 The high-frequency components of three-phase currents in case of an inter-turn fault ($\mu = 0.05$)

In order to classify the fault quantities from other components, the data vector must be transferred from X coordinates to D according to the formulations of PCA based on (14)—(17). Consequently, the decomposed vectors D_1, D_2, D_3, D_4, D_5 and D_6 are obtained. These are proportional to the descending order of the eigenvalues. For instance, the decomposition results of the stator three-phase currents in the case of an inter-turn fault ($\mu = 0.05$) according to Fig. 4 can be observed in Fig. 5. It is worth noting that the stator three-phase voltages can be used in other scenarios, such as voltage quality problems, in the same way.

To discriminate the SITF conditions from other conditions, the energy of the decomposed vectors is calculated according to (19) and the results are tabulated in Table 2. As shown in Table 2, the current energy of D_3 is the highest of all during an inter-turn fault, and the voltage energy of D_3 has the most presence of voltage quality problem source. Therefore, it can be concluded that the main source of the inter-turn and voltage quality problems signatures are present in D_3. In this way, the standard deviation of D_3 can be introduced as a criterion to separate the conditions.

$$E(D_j) = \sum_{k=1}^{N} \left[\frac{D_j[k]}{max(D_j)} \right]^2 \tag{17}$$

where $E(D_j)$, k and N denote the energy of the j-th decomposed vector, the number of samples, and the total number of decomposed vector's samples, respectively.

The standard deviation of D_3 is defined as the fault detection criterion, as:

$$\sigma_w = \sqrt{\frac{\sum_k^{Num}(x_{kw} - \varepsilon_w)}{Num}} \tag{18}$$

where σ_w, Num, x_{kw} and ε_w denote the standard deviation of the w-th data window, the number of window's samples, the k-th sample of the w-th data window, and the mean value corresponding to the w-th data window, respectively.

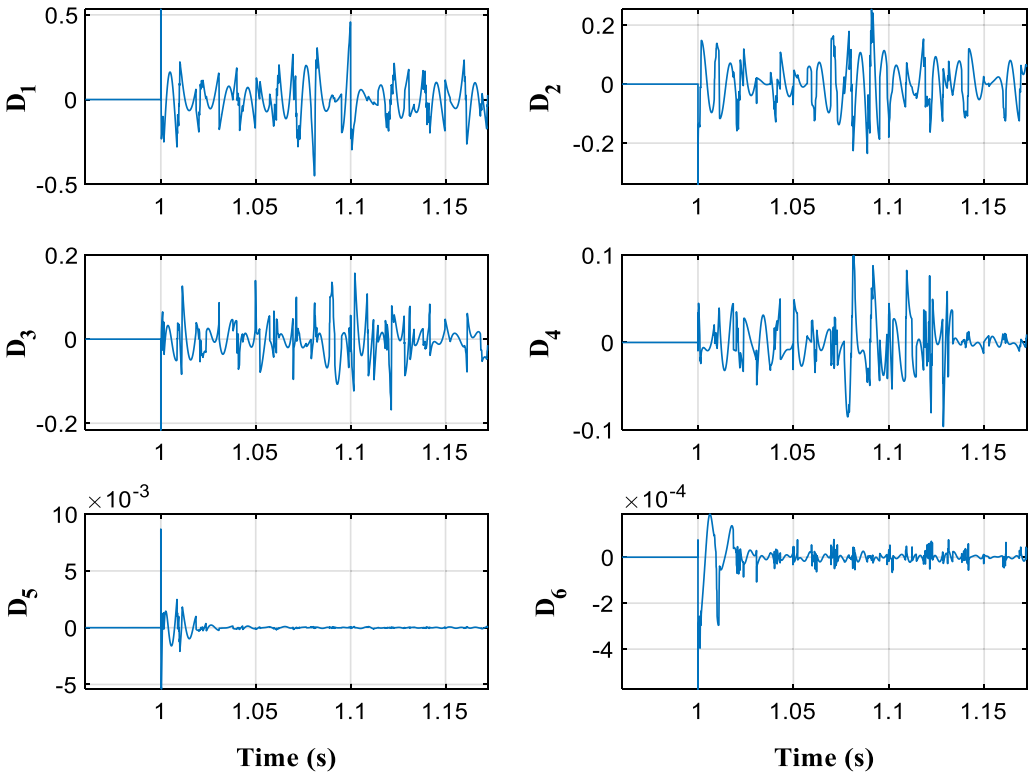

Fig. 5 The decomposition results of an inter-turn fault ($\mu = 0.05$), the largest eigenvalue is related to D_1 and the other components of three-phase stator currents are defined in the same arrangement

To prevent malfunction of the proposed criterion because of non-fault conditions such as voltage quality problems, the stator three-phase voltages, and the standard deviation of D_3 are used as inputs to the algorithm and auxiliary criterion, respectively.

One of the basic requirements of the proposed method is to define the thresholds for current and voltage criteria that have been selected based on large numbers of simulation and practical scenarios. In general, once the value of the current criterion is higher than its defined threshold while the voltage criterion does not exceed its predefined threshold, it can be considered as a fault condition. Whereas if both the current and voltage criteria are above their predefined thresholds, the algorithm identifies this condition as a voltage quality problem. If none of the voltage and current criteria reach their defined thresholds, it can be considered as a normal operating condition. The flowchart of the proposed method is presented in Fig. 6.

4 Simulation results for performance assessment of the proposed method

Simulation studies have great importance to the investigation into the dynamic fault behavior. Hence, a 1 kW three-phase IM with 220 V, 4 poles, and 50 Hz specifications based on (6)-(12) is simulated in MATLAB/SIMULINK. The considered scenarios in the simulation can be listed as follows:

- Inter-turn fault ($\mu = 0.05$)
- Voltage quality problems
- Voltage sag of 20%
- Voltage swell of 10%
- Unbalanced voltage of 2.64%
- Mechanical load changes from 0.7 to 1.5 pu
- Load rejection from 0.7 pu to no load

From Fig. 2, the current and voltage signals of the simulated IM in SIMULINK are gathered with a sampling frequency of 7812.5 Hz and are then passed through a high-pass filter with a cut-off frequency of 150 Hz. Then, by using two consecutive sliding windows each having a length of 156 samples (20 ms) and updated cycle by cycle, the matrix of X is created. Then, from (14)-(17) the decomposed vector D_3 is extracted. Finally, the standard deviation of D_3 is calculated. It is worth noting that both threshold values of Th_i and Th_v are selected as 0.01 based on the Otsu thresholding method [40], as well as experimental and simulation results in various cases including

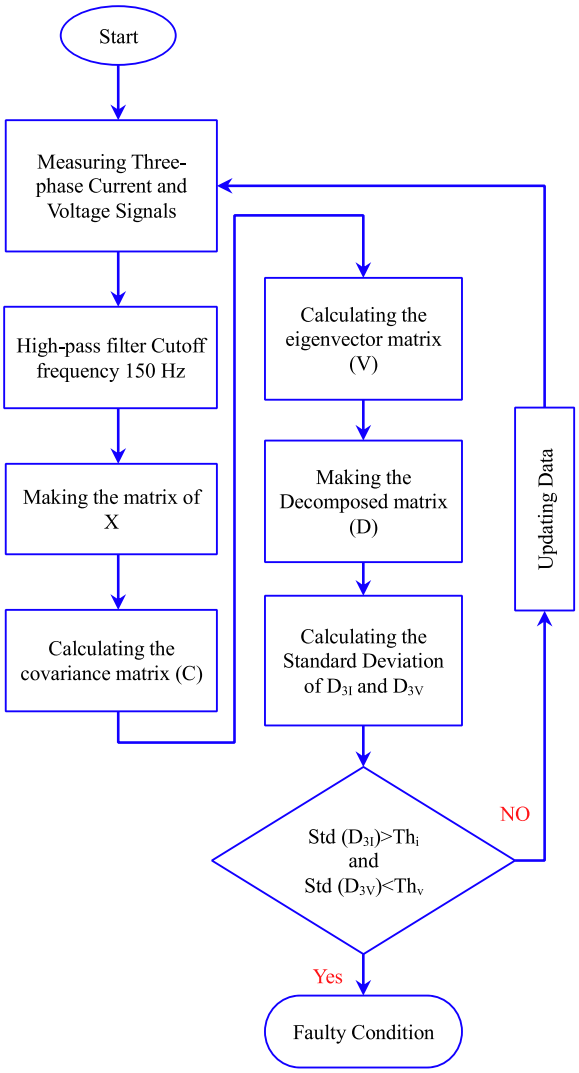

Fig. 6 The flowchart of the proposed method

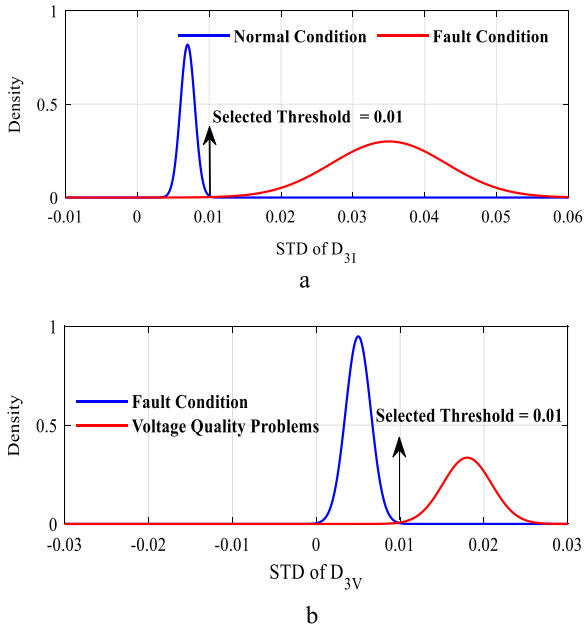

Fig. 7 The threshold selection process using Otsu thresholding method. **a** PDF curves of normal condition and fault condition for selecting a threshold value of current criterion, **b** PDF curves of voltage quality problem and fault condition for selecting a threshold value of voltage criterion

inter-turn fault, voltage quality problems, and mechanical load change.

As seen in Fig. 7a, the PDF curves of normal and fault condition have an intersection point at 0.01. Therefore, $Th_i = 0.01$ is a suitable threshold value in the current criterion for discriminating inter-turn fault from normal conditions. From the simulation and practical results, the performance of the current criterion is similar to voltage quality problems.

To prevent this malfunction, the voltage criterion is used as an auxiliary criterion. In a fault condition, the voltage criterion changes slightly compared to normal operating conditions, whereas in voltage quality problem cases, the voltage criterion changes significantly. Therefore, the Otsu thresholding method is used to differentiate the fault criterion changes from voltage quality problems by selecting an appropriate threshold. From Fig. 7b, $Th_v = 0.01$ can be seen as an appropriate threshold value in the voltage criterion for a robust performance against the voltage quality problems.

4.1 Inter-turn fault case

With μ as the fault severity, several inter-turn fault scenarios with μ between 0.02 and 0.1 are studied to evaluate the performance of the criteria. Here, only an inter-turn fault ($\mu = 0.05$) is presented as a typical case. In Fig. 8, the three-phase stator currents and voltages, as well as their corresponding high-frequency components and suggested criteria are demonstrated.

As can be observed in Fig. 8a, by applying an inter-turn fault at $t = 1s$, the three-phase currents are changed and become unbalanced. It is clear from Fig. 8b that because of the occurrence of the fault, some high-frequency components have been created in the three-phase currents. By extracting the decomposed vector D_3 and calculating its standard deviation in Fig. 8c, a sudden increase in the current criterion occurs and reaches 0.058 units from zero and exceeds its predefined threshold of 0.01. In a similar side of the algorithm according to Figs. 8d-f, the three-phase voltage signals have small changes and the standard deviation varies fractionally from 0 to 0.0001 indicating a very significant difference from the threshold of 0.01.

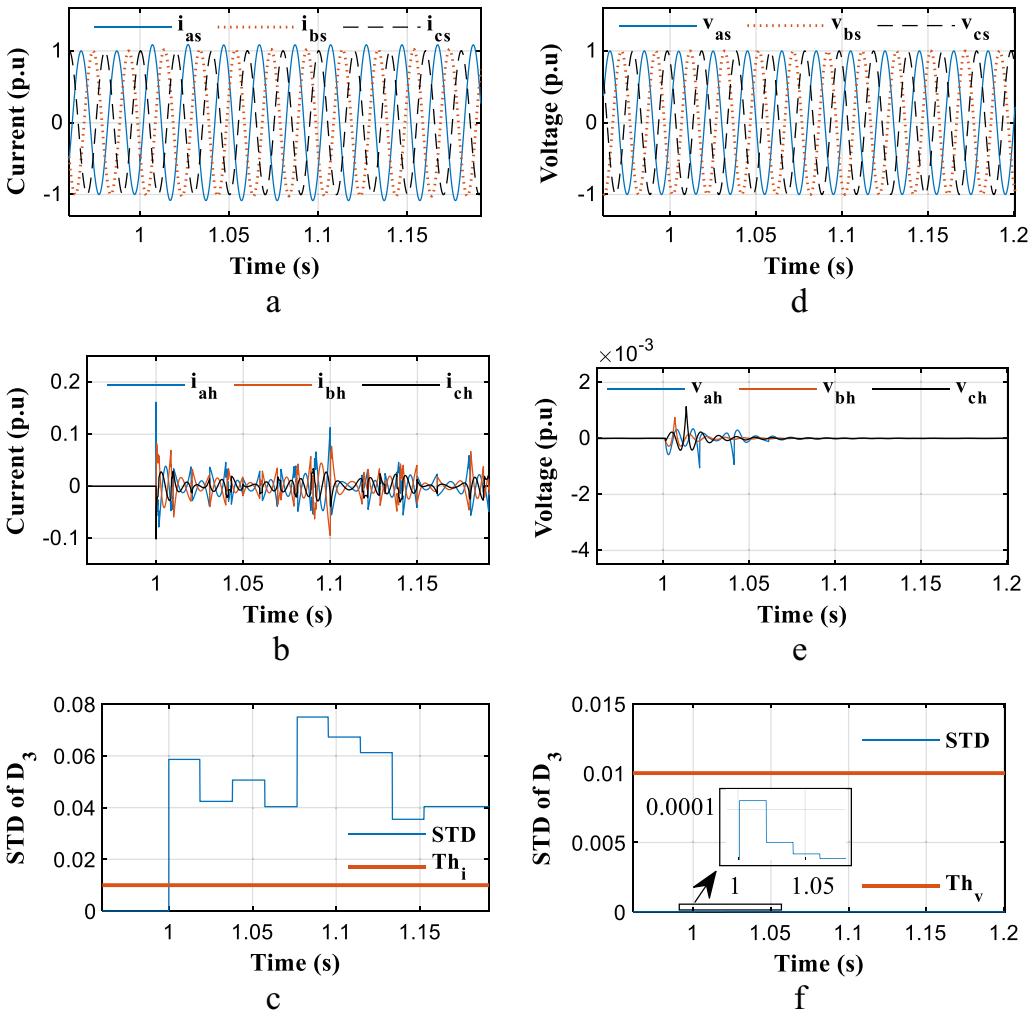

Fig. 8 Performance evaluation of proposed criteria using simulation results for an inter-turn fault ($\mu = 0.05$), **a** Three-phase stator current signals, **b** High-frequency components of three-phase stator current signals, **c** The current criterion, **d** Three-phase stator voltage signals, **e** High-frequency components of three-phase stator voltage signals, **f** The voltage criterion

In practice, some unwanted harmonic components may result in harmonic contamination in the voltage supply. Therefore, the performance of the proposed criteria should be investigated before and after the fault occurrence. Since the general basis of the suggested criteria is on the distortion of the measured signal after the disturbance, for studying the ability of the proposed algorithm in presence of voltage supply contaminated with high-order harmonic components several case studies are considered. Different levels of total harmonic distortions *THD* s between 1 and 5% are fed to the voltage supply. Here, to detect the coil-to-coil fault ($\mu = 0.1$) considering 5% *THD* in the voltage supply, the performance of the algorithm is investigated. It can be observed from Fig. 9b that before $t = 1s$, because of the harmonic contamination in the voltage supply, there are some high-frequency components in the three-phase stator currents. According to Fig. 9c, although the value of the current criterion is not zero and is equal to 0.001, it is significantly lower than 0.01. This indicates a strong performance against harmonic pollution in the voltage supply up to $THD = 5\%$. On the other side, from Fig. 9d, the three-phase voltage signals are out of sinusoidal form because of harmonic contamination in the voltage supply. Consequently, as shown in Fig. 9f, the value of the pre-fault voltage criterion is approximately 0.002. At the moment of $t = 1s$, the voltage criterion value reaches 0.005 which is lower than its predefined threshold. It is worth mentioning that a higher THD can be dealt with by re-adjusting the thresholds.

4.2 Voltage quality problems case

There is a serious impact of non-fault transient conditions on the performance of Ims. Thus the performance

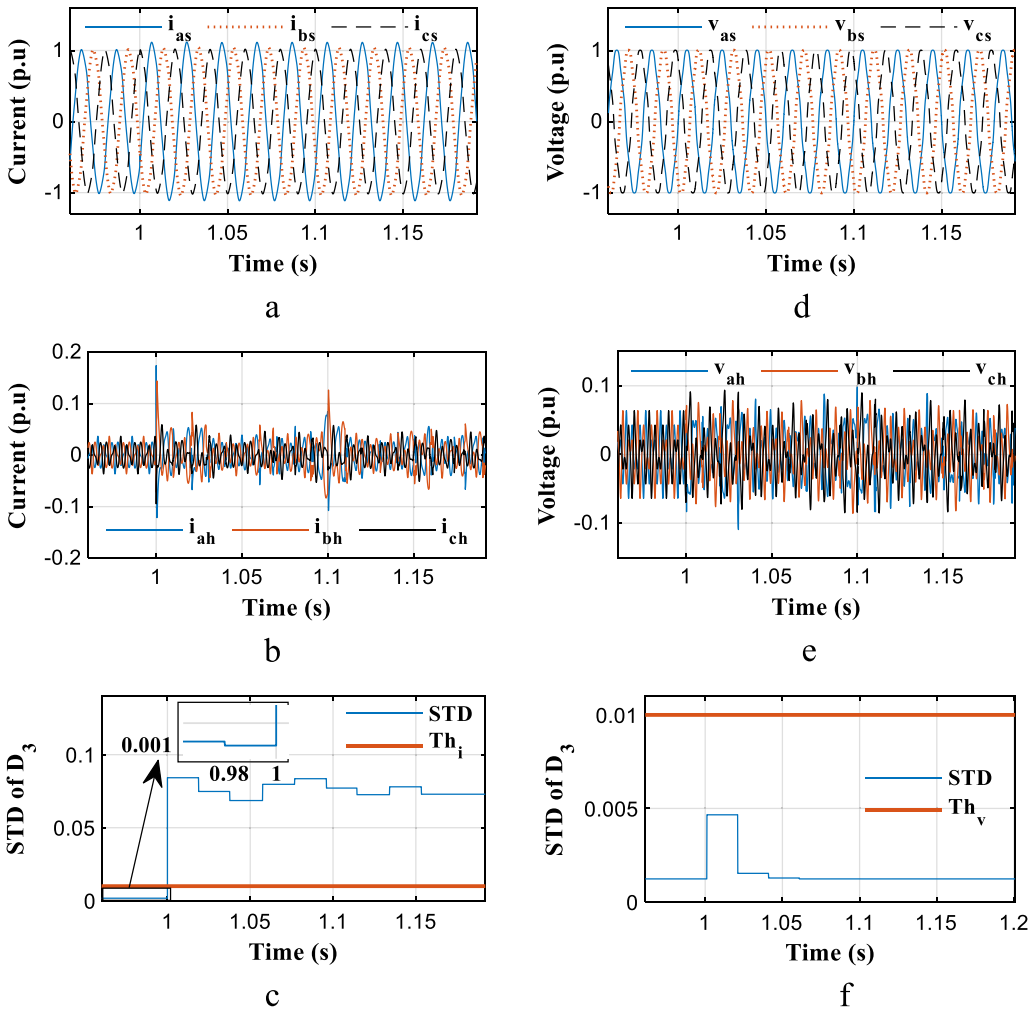

Fig. 9 Performance evaluation of proposed criteria using simulation results for a coil-to-coil fault ($\mu = 0.1$) in a voltage distortion with $THD = 5.2\%$, **a** Three-phase stator current signals, **b** High-frequency components of three-phase stator current signals, **c** The current criterion, **d** Three-phase stator voltage signals, **e** High-frequency components of three-phase stator voltage signals, **f** The voltage criterion

of the proposed criteria under the most common transient conditions that may create overlap with inter-turn fault conditions must be evaluated. Hence, the performance of the proposed criteria under voltage sag and swell are investigated in this section. Figures 10 and 11 depict the simulation results for voltage sag of 20% and voltage swell of 10%.

In Fig. 10, a voltage sag of 20% happens for 5 cycles. As seen in Fig. 10d, the three-phase voltages are decreased from 1 pu to 0.8 pu at $t = 1s$ resulting in the current and voltage criteria increasing to 0.0105 and 0.012 units as seen in Fig. 10c–f, respectively. It is interesting to note that both the current and voltage values of the criteria exceed their corresponding predefined thresholds and the proposed algorithm identifies this condition as a voltage quality problem.

As presented in Fig. 11d, a voltage swell of 10% occurs at time interval of $t = 1s$ to $t = 1.1s$ and the three-phase voltages increase from 1 pu to 1.1 pu. Because of the voltage swell occurrence, the current criterion has increased approximately to 0.015 in Fig. 11c and as observed in Fig. 11f, there is a growth to around 0.012 in the voltage criterion.

One of the most frequent voltage quality problems is voltage imbalance in the supply. In this section, an unbalanced supply voltage of 2.64% is investigated, and the simulation results are presented in Fig. 12. It should be noted that the voltage imbalance is defined according to [41]:

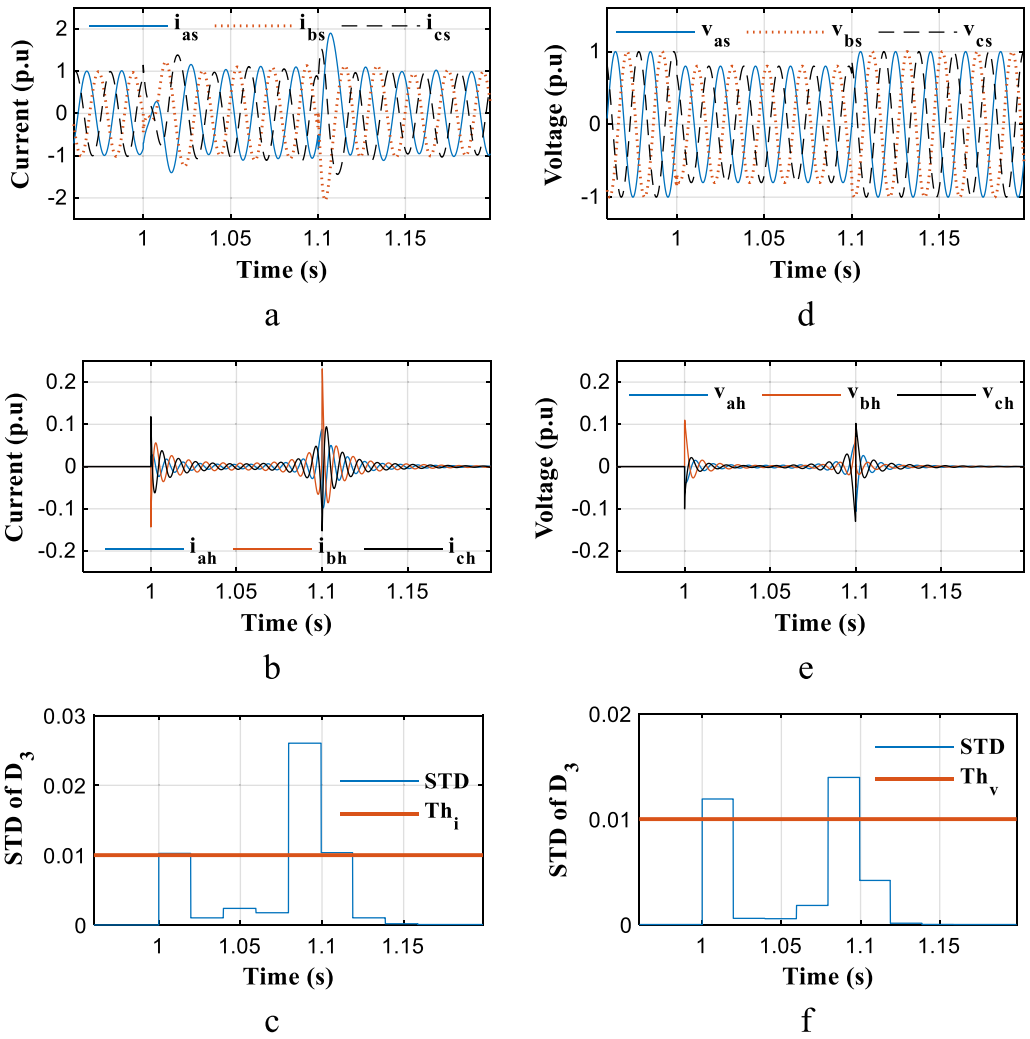

Fig. 10 Performance evaluation of the proposed criteria using simulation results for a voltage sag of 20%, **a** Three-phase stator current signals, **b** High-frequency components of three-phase stator current signals, **c** The current criterion, **d** Three-phase stator voltage signals, **e** High-frequency components of three-phase stator voltage signals, **f** The voltage criterion

$$\textit{voltage imbalance} = \frac{\textit{maximum deviation from average phase voltage}}{\textit{average phase voltage}} \times 100 \quad (19)$$

Figure 12d shows that the stator voltages of phases a, b, and c change from 1 p.u to 1.02 p.u, 0.98 p.u, and 0.98 p.u respectively, and the three-phase stator currents are out of equilibrium. As a result, both the current and voltage criteria based on Fig. 12c–f reach 0.015 and 0.0104 respectively. These exceed the predefined thresholds.

4.3 Mechanical load changes case

In this section, we investigate the performance of the criteria when there is mechanical load change. A mechanical load increase from 0.7 to 1.5 pu is shown in Fig. 13. Although the three-phase stator currents increase significantly from 1 to 2 pu, the current criterion value is approximately 0.0001 while the voltage criterion value is less than 0.00001, as seen in Fig. 13c–f Both are less than their defined thresholds, and thus the proposed algorithm considers it as a normal operating condition.

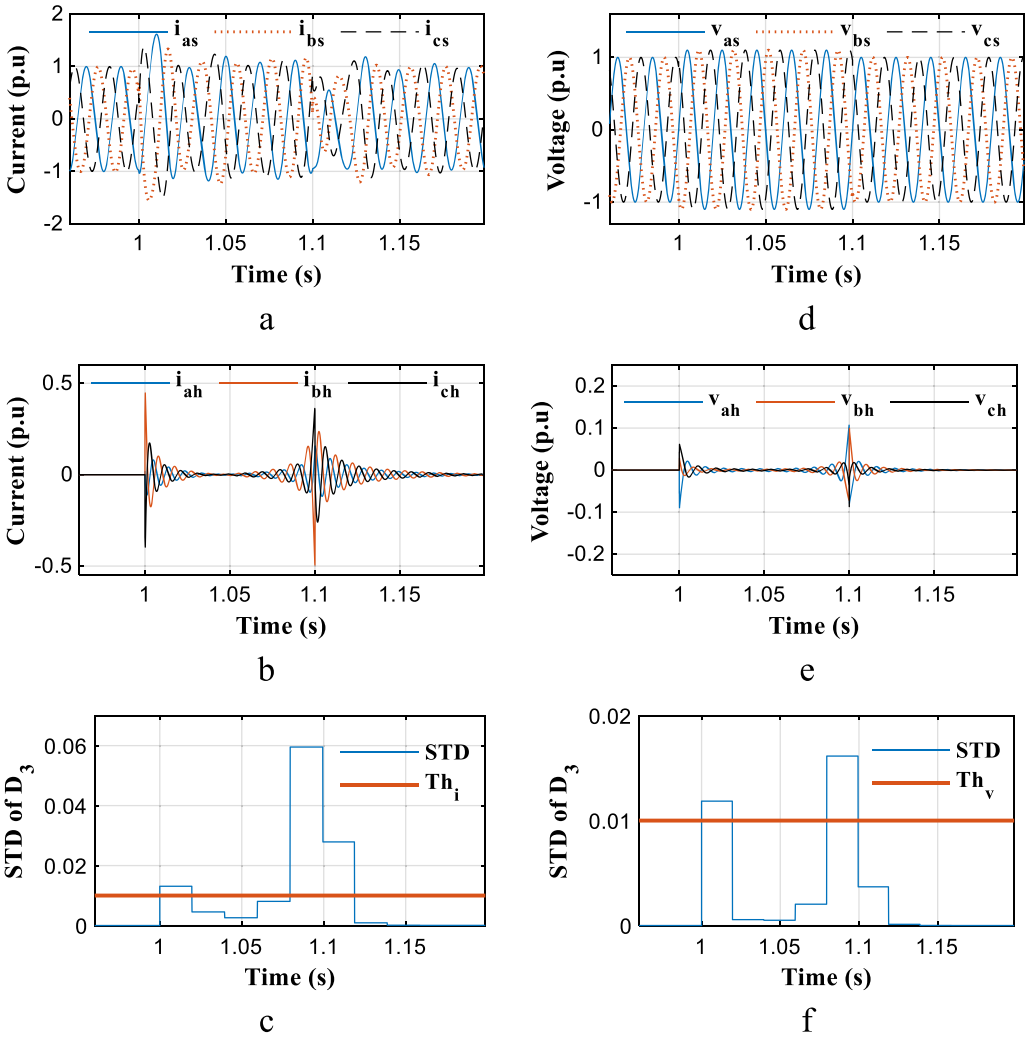

Fig. 11 Performance evaluation of proposed criteria using simulation results for a voltage swell of 10%, **a** Three-phase stator current signals, **b** High-frequency components of three-phase stator current signals, **c** The current criterion, **d** Three-phase stator voltage signals, **e** High-frequency components of three-phase stator voltage signals, **f** The voltage criterion

4.4 Load rejection case

Another transient condition which can profoundly affect the performance of IMs is load rejection. Load rejection phenomena occur differently in generators, where the rejection of the load means the rejection of power whereas in motors it means the mechanical load is rejected. As load rejection in generators affects the electromagnetic environment, it is important to evaluate the performance of the proposed criteria where load rejection may create ambiguity in the inter-turn fault conditions. In the following, the performance of the proposed criteria under a load rejection from 0.7 pu to no load at t = 1 s is investigated. As shown in Fig. 14a, after the occurrence of the rejection, the three-phase stator currents fluctuate from 1 pu to 0.8 pu and subsequently the current criterion increases to 0.007. From the other side, as shown in Fig. 14d, the three-phase stator voltages increase slightly from 1 pu to 1.08 pu and the voltage criterion also is significantly less than its threshold value (0.01) according to Fig. 14f.

As neither criterion exceeds the corresponding threshold values the proposed algorithm does not maloperate in this condition.

5 Practical results for assessment of the suggested method

To validate the simulation results and the proposed methodology, an experimental platform is implemented as shown in Fig. 15. This experimental bench consists of a three-phase IM with its specifications listed in Table 3, a data logger for recording the MCS and MVS

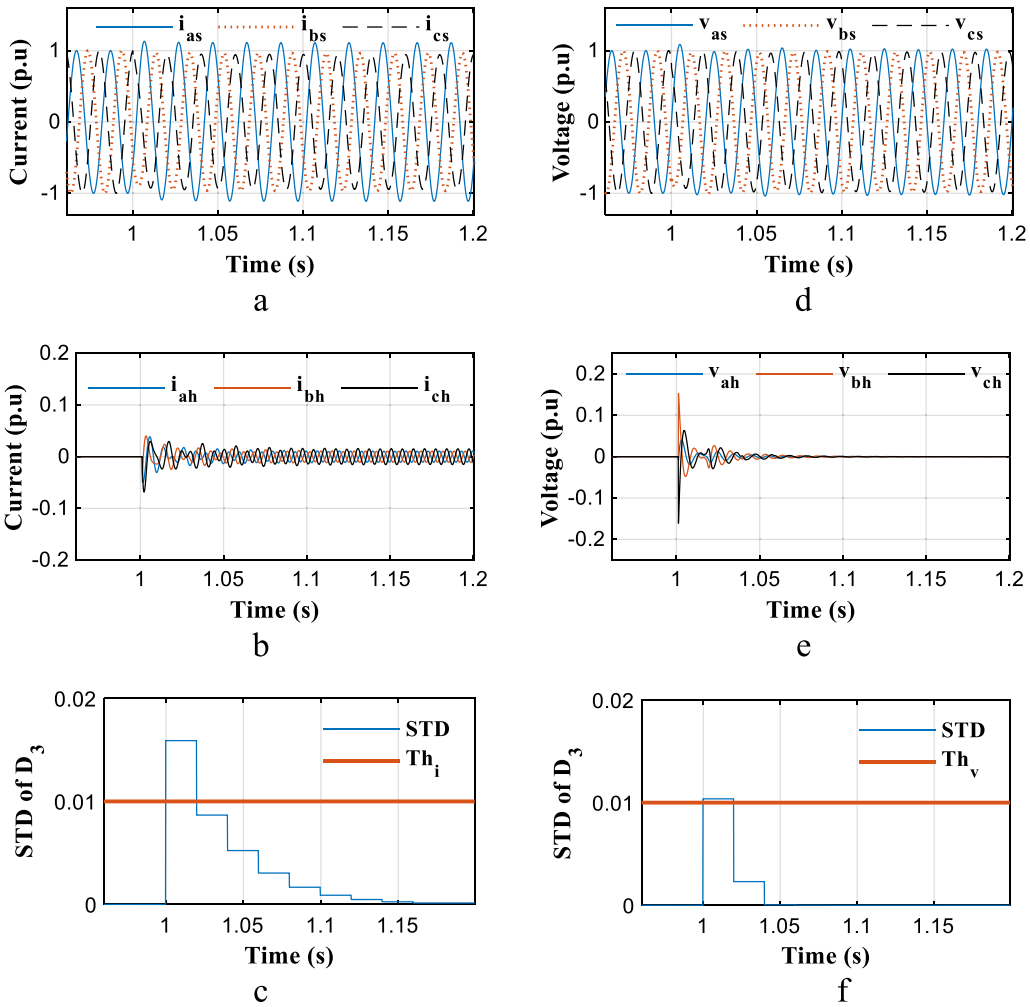

Fig. 12 Performance evaluation of proposed criteria using simulation results for an unbalance voltage of 2.64%, **a** Three-phase stator current signals, **b** High-frequency components of three-phase stator current signals, **c** The current criterion, **d** Three-phase stator voltage signals, **e** High-frequency components of three-phase stator voltage signals, **f** The voltage criterion

with sampling time of 128 μs, a coupled DC machine with different mechanical load torques for IM, and a three-phase autotransformer as a variable voltage supply. The practical scenarios can be summarized as:

- Inter-turn fault ($\mu = 0.05$)
- Voltage quality problems
- Voltage sag of 20%
- Voltage swell of 10%
- Unbalanced voltage of 2.8%
- Mechanical load changes from 0.7 to 1.5 p.u

For implementing voltage quality problems such as voltage sag and swell, two controllable and uncontrollable methods have been used. The meaning of controllable is the use of 3 autotransformers for regulating voltages of the motor. Using the controllable method, motor supply voltages can be increased or decreased to the desired value over a certain time period, but the uncontrollable method can be implemented by starting a large motor in parallel with the test motor and turning off the large parallel motor load that is fed from the voltage source respectively. In unbalanced voltage, the controllable method is also used and an unbalanced three-phase source has been created by this method. It should be noted that most scenarios of voltage quality problems have been implemented based on the controllable method although uncontrollable methods have been used to show the flexibility of the proposed algorithm. Figures 16, 17, 18, 19, 20 depict the practical results of different cases. These consist of inter-turn fault, voltage quality problems and mechanical load

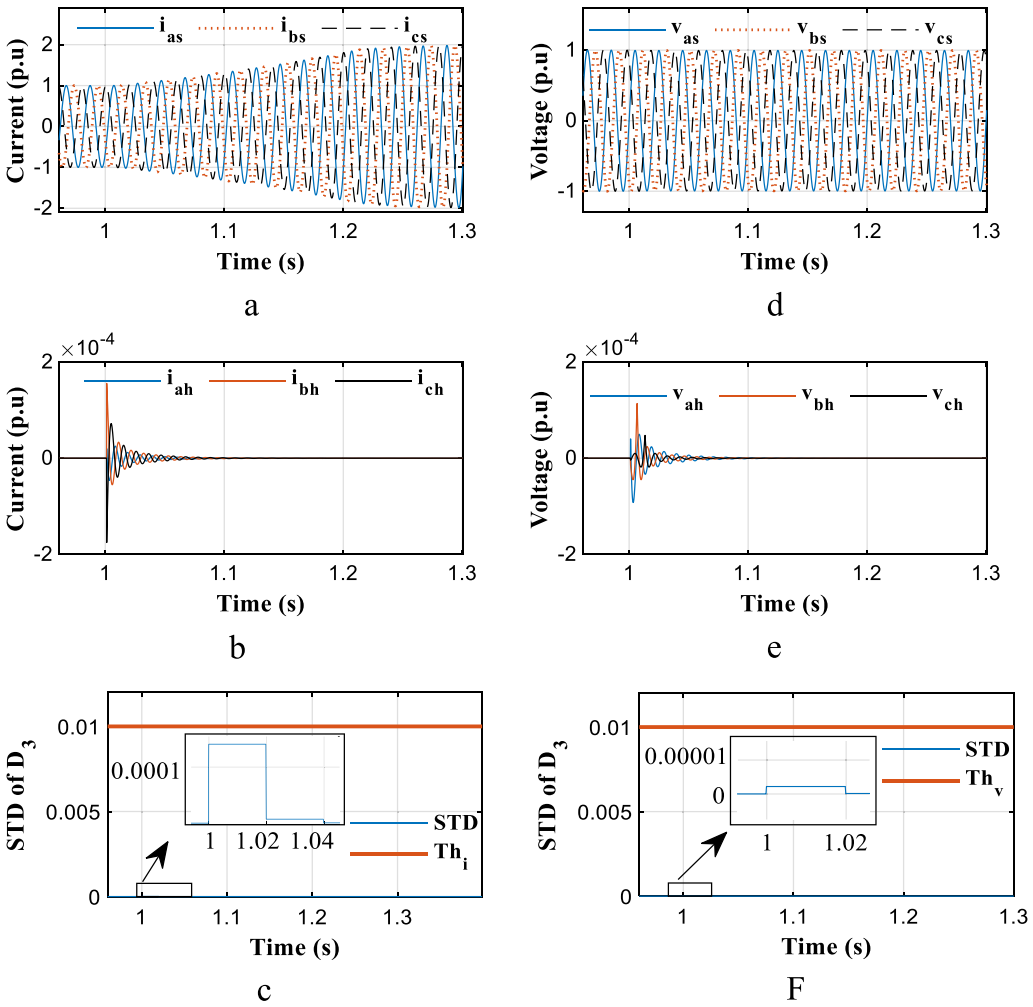

Fig. 13 Performance evaluation of proposed criteria using simulation results for a mechanical load change of 80%, **a** Three-phase stator current signals, **b** High-frequency components of three-phase stator current signals, **c** The current criterion, **d** Three-phase stator voltage signals, **e** High-frequency components of three-phase stator voltage signals, **f** The voltage criterion

changes. From Fig. 16, it can be clearly seen that the simulation results results are confirmed and because of the fault occurrence, some high-frequency components are created at $t = 0.53s$ as.

indicated in Fig. 16c–f. The current criterion value increases dramatically from 0.006 to 0.04 whereas the voltage criterion value remains approximately stable at 0.005. The values of the current and voltage criteria are higher and lower than their corresponding thresholds. As can be seen, the practical results are largely identical to the simulation results, and the suggested algorithm recognizes this as a faulty condition.

Figures 17, 18, 19 illustrate the results of some non-fault scenarios such as voltage sag, voltage swell and unbalanced supply voltage. In Fig. 17c, a voltage sag occurs at $t = 0.62s$ and the current and voltage criteria in Fig. 17b–d reach 0.021 and 0.02, respectively, which exceed the threshold of 0.01.

A voltage swell of 10% happens for 10 cycles resulting in an abrupt change of the high-frequency components of the voltage and current signals, and are similar to corresponding scenarios in simulation. Because of the sudden changes, both criteria have exceeded their defined threshold values as shown in Fig. 18b–d.

In the next step, the results of an unbalanced voltage of 2.8% as one of the possible voltage quality problems is investigated in Fig. 19. As seen in Fig. 19c, the voltage imbalance is applied at $t = 0.66s$ and the stator voltages of phases a, b and c change from 1 to 1.03 pu, 0.95 pu,

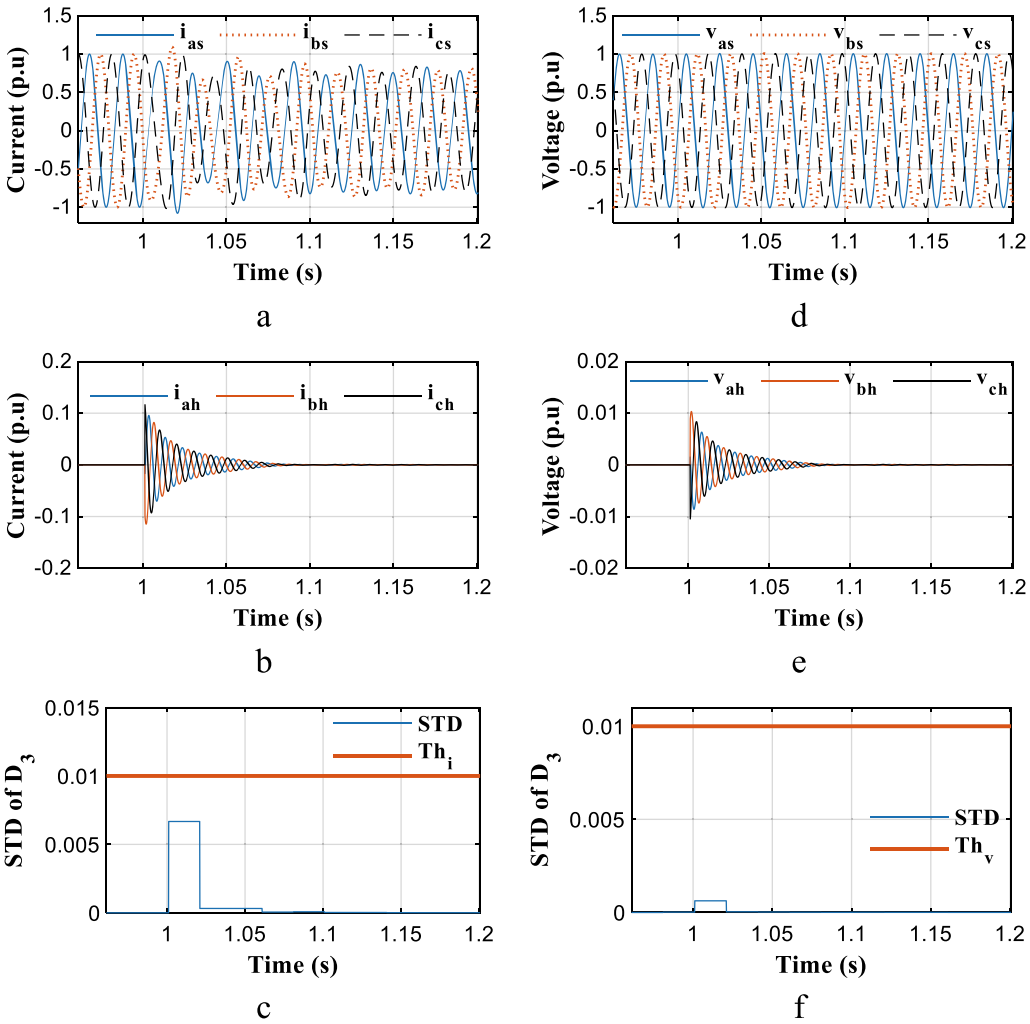

Fig. 14 Performance evaluation of proposed criteria using simulation results for a load rejection from 0.7 p.u to no load, **a** Three-phase stator current signals, **b** High-frequency components of three-phase stator current signals, **c** The current criterion, **d** Three-phase stator voltage signals, **e** High-frequency components of three-phase stator voltage signals, **f** The voltage criterion

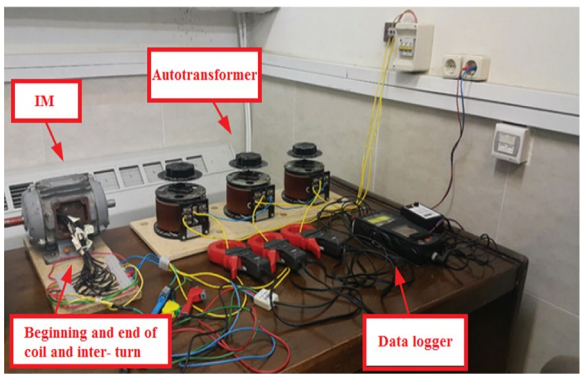

Fig. 15 Implemented experimental platform for detecting SITF

Table 3 Specification of IM used

Symbol	Quantity	Value
P_n	Nominal power	1 KW
V_{abc}	Rated voltage	220 V
I_{abc}	Rated current	3.6 A
f_s	Rated frequency	50 Hz
$cos(\emptyset)$	Rated power factor	0.74
J	Rotor inertia	0.0025 Kg m^2
P	Number of poles	4
ω_r	No load speed	145.0368 rad/s
R_s	Stator winding resistance	8.4 Ω
R_r	Referred rotor winding resistance	8.2 Ω
L_{ls}	Stator winding leakage inductance	32.78 mH
L_{lr}	Referred rotor winding leakage inductance	32.78 mH
L_m	Magnetizing inductance	437.67 mH

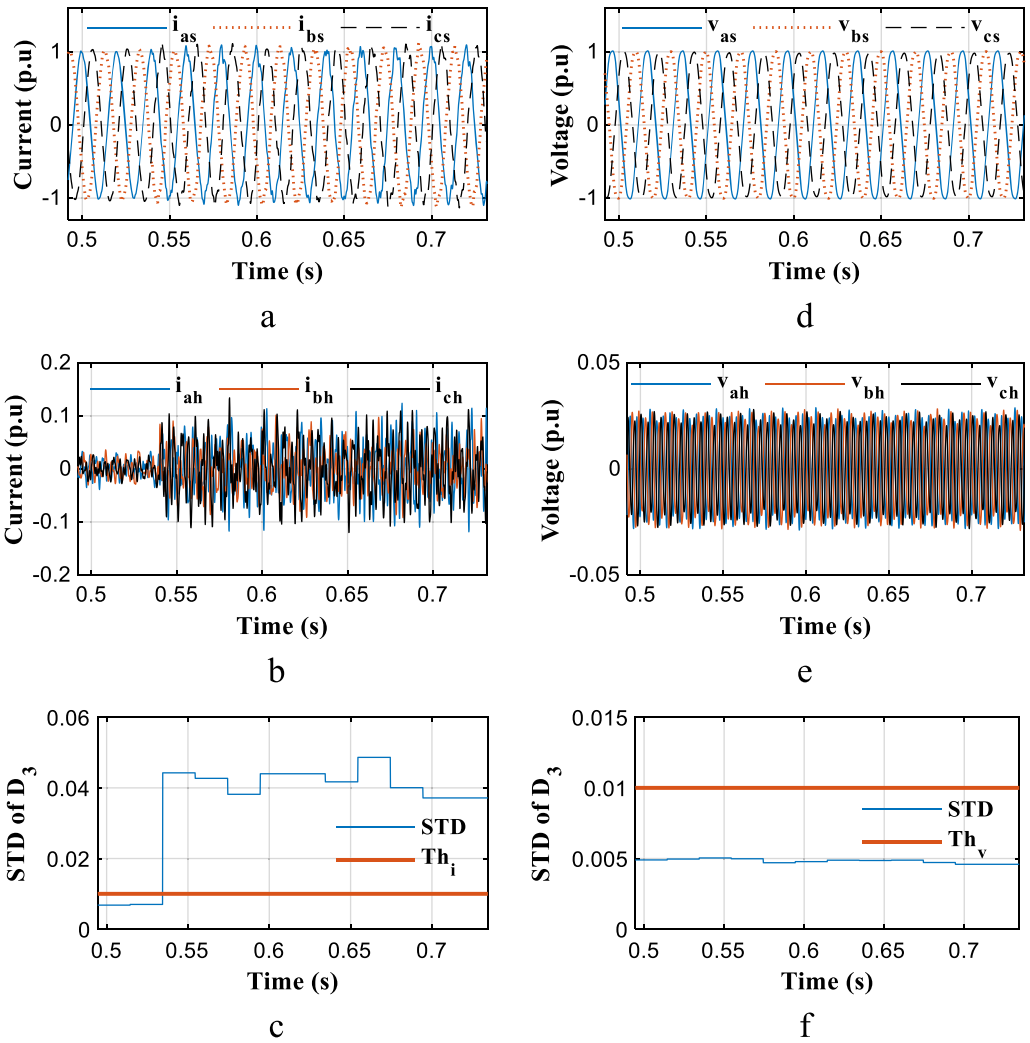

Fig. 16 Performance evaluation of proposed criteria using practical results for an inter-turn fault ($\mu = 0.05$), **a** Three-phase stator current signals, **b** High-frequency components of three-phase stator current signals, **c** The current criterion, **d** Three-phase stator voltage signals, **e** High-frequency components of three-phase stator voltage signals, **f** The voltage criterion

respectively. It is evident that the current and voltage criteria increase from 0.007 and 0.005 to 0.017 and 0.012 respectively, with both criteria crossing their corresponding threshold values in Fig. 19b–d.

As a general trend based on the simulation and practical results, both the current and voltage criteria exceed their defined threshold values when a voltage quality problem occurs.

Finally, the practical results of mechanical load changes are presented in Fig. 20. In this case, the three-phase currents increase gradually from 1 to 2 pu, while according to Fig. 20c–f, the values of the current and voltage criteria are both less than 0.01.

6 Robustness of the criteria against parameter variation

In this section, the flexibility of the algorithm considering the effects of different parameters, such as fault resistance, harmonic contamination in the supply voltage, mechanical load change rate and noise, are evaluated.

6.1 Effect of fault resistance

The results of the proposed criterion in the case of inter-turn faults with different intensities for changes in fault resistance from 0 to 2000 Ω are tabulated in Table 4.

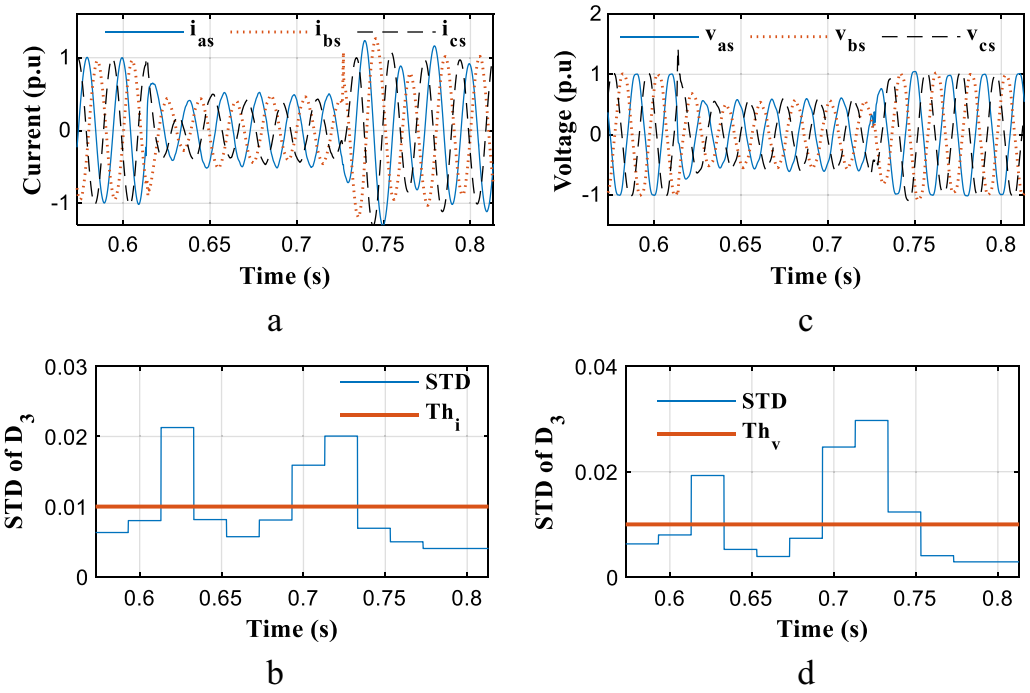

Fig. 17 Performance evaluation of proposed criteria using practical results for a voltage sag 20%, **a** Three-phase stator current signals, **b** The current criterion, **c** Three-phase stator voltage signals, **d** The voltage criterion

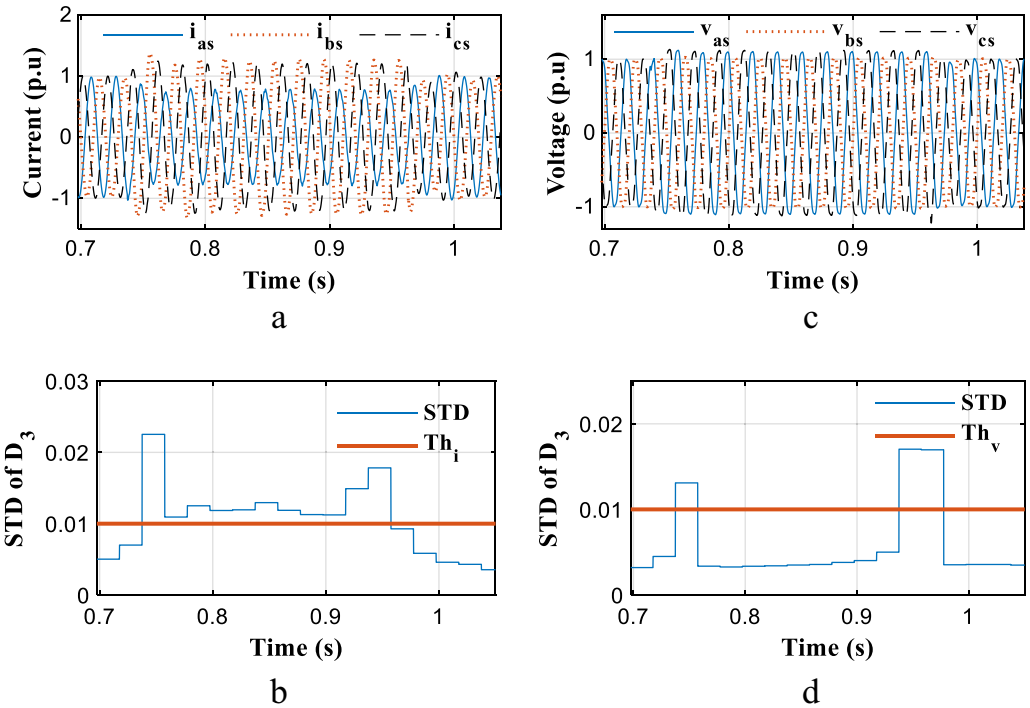

Fig. 18 Performance evaluation of proposed criteria using practical results for a voltage swell 10%, **a** Three-phase stator current signals, **b** The current criterion, **c** Three-phase stator voltage signals, **d** The voltage criterion

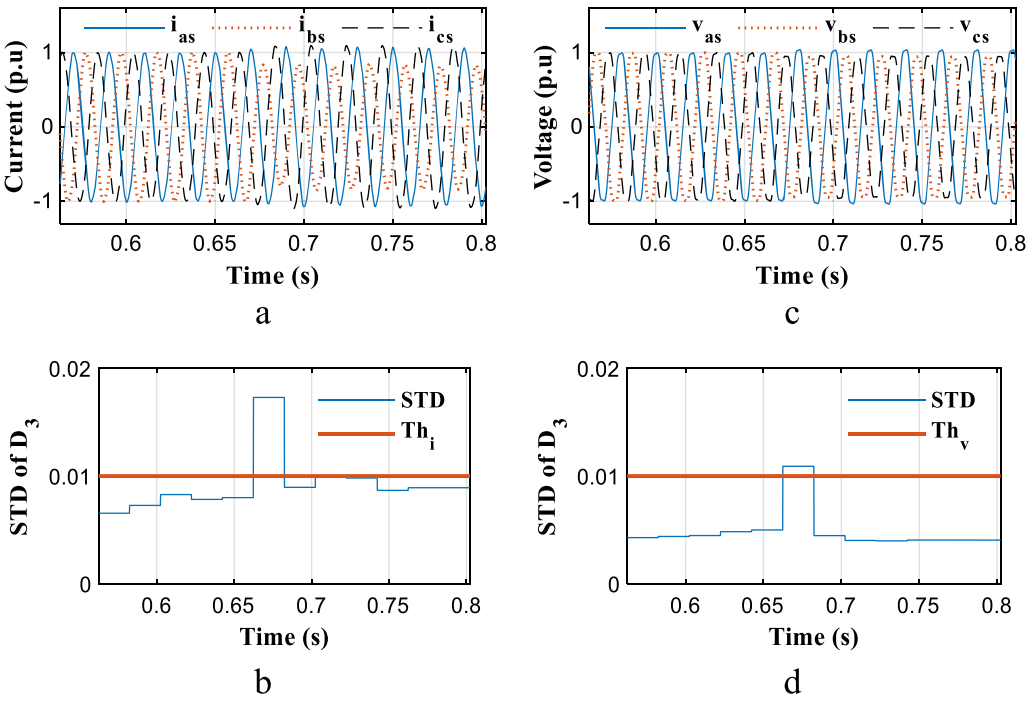

Fig. 19 Performance evaluation of proposed criteria using practical results for a voltage swell 10%, **a** Three-phase stator current signals, **b** The current criterion, **c** Three-phase stator voltage signals, **d** The voltage criterion

As shown in Table 4, for changes in fault resistance from 0 to 1 Ω, the values of the current criterion are largely the same. For instance, in the inter-turn fault ($\mu = 0.05$), the current criterion values are approximately 0.055 whereas at a higher value of fault resistance (100Ω), the criterion decreases to 0.041 and this downward trend of the current criterion is continued for increase in the fault resistance to the values as high as thousands of ohms. As an illustration of this downward trend, at a fault severity of 0.05 and fault resistance of 1000 Ω, the current criterion is significantly reduced to 0.029, while for a fault resistance 2000 Ω, it reaches 0.023. From this perspective, notwithstanding this proximity to the margin value of the current criterion threshold (0.01) at high fault resistance, the proposed method is still robust for fault resistances as high as thousands of ohms.

The performance of the proposed criterion for the other fault intensities such as inter-turn fault ($\mu = 0.02$), inter-turn fault ($\mu = 0.07$) and a coil-to-coil fault ($\mu = 0.1$) are also investigated. As can be seen, the value of the current criterion in each fault resistance increases with increasing fault intensity. For instance, at $R_f = 1000\Omega$, with fault intensity increasing from 0.02 to 0.1, the values of the criterion increase from 0.02 to 0.047. Consequently, the proposed algorithm is robust against different fault resistances considering different fault intensities. It should be noted that the results in Table 4 are reported based on 1280 different simulation cases and 450 different experimental cases.

6.2 Effect of harmonic supply voltage contamination

As discussed, under normal conditions, both the current and voltage criteria are less than 0.01. At the moment of fault inception, the current criterion exceeds its predefined threshold whereas the voltage criterion remains below 0.01. Accordingly, if the voltage supply is contaminated with unwanted harmonics, the value of the current criterion before the fault inception and the value of the voltage criterion after the fault occurrence may cross their corresponding thresholds. This will eventually lead to maloperation of the proposed algorithm. Therefore, it is necessary to ensure that harmonic contamination will not result in maloperation of the algorithm. The results of this case are presented in the form of a line graph for an increase of *THD* from 0.3 to 10.5% in Fig. 21. Δ_i denotes the distance between the threshold and current criterion before the disturbance inception while Δ_v is the distance between the threshold and voltage criterion after the fault occurrence.

From Fig. 21, it is clear that Δ_i and Δ_v remain almost constant with the increase of *THD* from 0.3 to 3.12%, but from $THD = 3.12\%$ onwards, Δ_v has a steeper downward slope than Δ_i. At $THD = 9.4\%$, Δ_v is negative, but Δ_i remains positive. Finally, at $THD = 10.5\%$, both Δ_i and

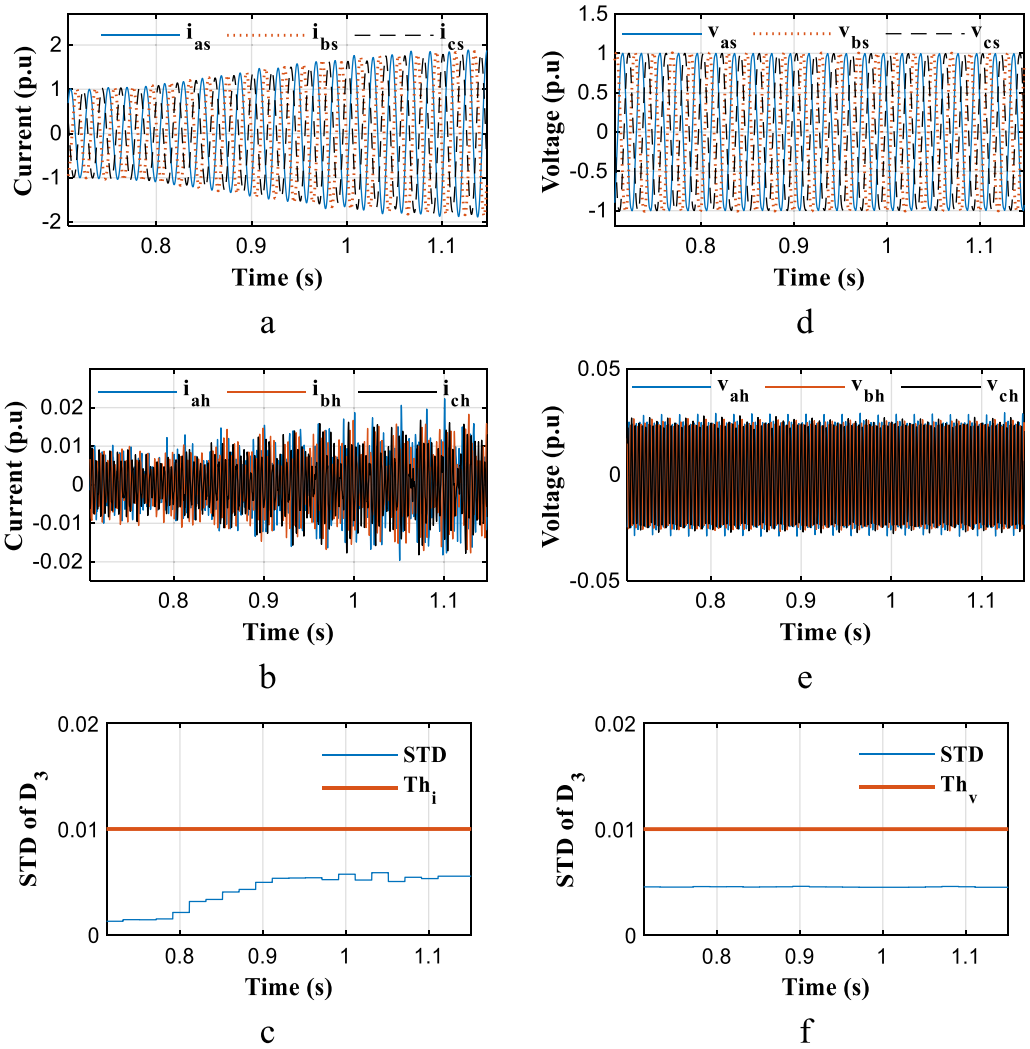

Fig. 20 Performance evaluation of proposed criteria using practical results for a mechanical load change 80%, **a** Three-phase stator current signals, **b** High-frequency components of three-phase stator current signals, **c** The current criterion, **d** Three-phase stator voltage signals, **e** High-frequency components of three-phase stator voltage signals, **f** The voltage criterion

Table 4 Average current criterion value for different fault resistance

μ	$R_f(\Omega)$					
	0	**0.01**	**1**	**100**	**1000**	**2000**
0.02	0.044	0.041	0.039	0.029	0.02	0.015
0.05	0.058	0.055	0.053	0.041	0.029	0.023
0.07	0.067	0.063	0.06	0.048	0.041	0.036
0.1	0.081	0.079	0.076	0.055	0.047	0.039

Δ_v are negative. Here, the permissible *THD* in which the method can preserve its desirable robustness and performance is considered to be 5.2%. However, the proposed algorithm can perform adequately for *THD* up to 8.8%.

6.3 Effect of mechanical load changes

As mentioned earlier, both the current and voltage criteria values are less than their thresholds in the mechanical load change conditions. The results of different load

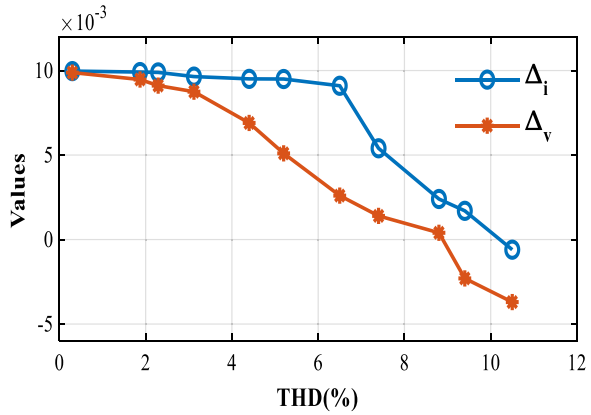

Fig. 21 Harmonic contamination effect on proposed criteria

changes are listed in Table 5. $T_{L1}(p.u)$ and $T_{L2}(p.u)$ denote the load values before and after changes. It is evident that all values of the current criterion are less than 0.01 and as a result, this scenario can be considered as normal operating conditions.

6.4 Effect of Gaussian Noise

Typically, the measured signals in the power system are contaminated with noise. Hence, the performance of the proposed criteria in the presence of Gaussian noise is assessed and the results are shown in Table 6, where P_s and P_n denote the power of the signal and noise, respectively. As observed, with decrease of SNR from 60 to 30db, both Δ_i and Δ_v decrease, and at SNR = 30db, Δ_v becomes negative. Although the value of Δ_i is positive, it is, and voltage criteria are both less than 0.01.

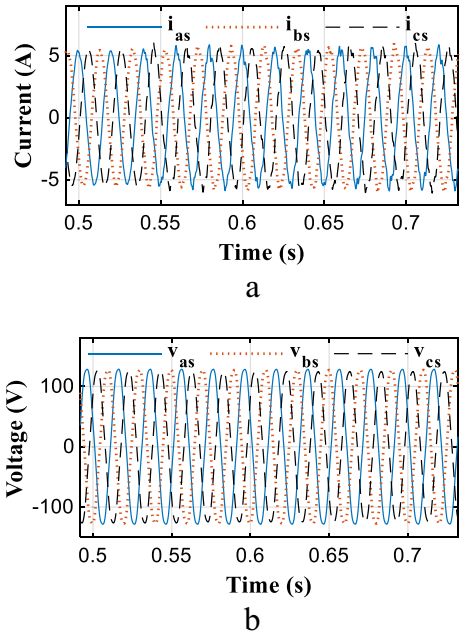

Fig. 22 The accurate working values of CT and PT. **a** Three-phase stator currents, **b** Three-phase stator voltages

7 Experimental implementation requirements and factors affecting accuracy

As described in the Introduction, signal-based methods are divided into invasive and non-invasive. Given that the proposed method is a non-invasive one, only the effects of faults in the stator current and voltage or other obtainable electrical quantities are used as a fault criterion and there is no need to install an additional sensor on the motor [6]. In this method, the measured currents and

Table 5 Current criteria value in different mechanical load changes

$T_{L1}(p.u)$	0.7	0.2	0.6	0.5	0.6	0.3
$T_{L2}(p.u)$	1.5	0.6	0.9	1	1.3	0.9
Current criterion value	0.0026	0.0013	0.001	0.0016	0.0021	0.0019

Table 6 White noise effect on proposed criteria

	SNR(db) = 10log(P_s/P_n)					
	60	55	50	45	40	30
Δ_i	0.0099	0.0085	0.007	0.005	0.003	0.001
Δ_v	0.0098	0.0087	0.005	0.0024	0.0017	-0.004

Table 7 Comparison of the proposed method with similar methods based on MCS and MVS

	Comparative aspects				
	Analyzing domain	**The required signals**	**Delay time (s)**	**Average accuracy percentage (%)**	**Robustness to voltage quality problems**
[42]	t	I-V	0.02	79	Yes
[19]	t-f	I-V	0.01	81	Yes
[16]	t-f	I	0.02	84	No
[17]	t-f	I	0.02	90	No
Proposed method	t-f	I-V	0.02	94	Yes

voltages from the current transformer (CT) and potential transformer (PT) are used. The requirements of the proposed method in experiments are CT, PT and an algorithm in a computer or implemented in hardware for analyzing the behavior of the motor.

In the experiments, the current and voltage signals are measured with a Lutron DL-9954 (clamp meter), with voltage resolution and accuracy of 0.1 V and 1.2% respectively, current resolution and accuracy of 0.01 A and 1.5% respectively, and a data logger with a sample rate of 128 μs. As an example, the accurate working values of CT and PT in an inter-turn fault with $\mu = 0.05$ are illustrated in Fig. 22. As shown in Fig. 22a, when an inter-turn fault occurs at $t = 0.53s$, the three-phase currents increase approximately from 5 A to 5.9 A while the three-phase voltages go from 127 to 130 V.

Some factors can affect the accuracy and even cause the proposed criteria to maloperate, e.g.: (1) use of a CT and PT with improper accuracy class; (2) unsuitable selection of turns ratio regardless of motor power and voltage level; and (3) CT and PT saturation.

8 Performance comparison between the proposed strategy and several state-of-the-art techniques

In Table 7, the proposed approach is compared with several other methods from the aspects of delay time, analyzing domain, the required signals, average accuracy, and robustness to voltage quality problems. The other techniques are selected based on MCS and MVS for an equitable comparison.

From Table 7, the difference between the calculated equivalent impedance and its reference value is presented as a fault criterion. Although robustness to voltage quality problems can be seen in [42], its biggest drawback, however, is the lowest average accuracy based on abundant simulations and experimental results compared to the other methods. Reference [19] has the best time delay in comparison to the other methods, but it has insufficient accuracy for detecting faults, and is affected by selecting the appropriate window length in FFT-based methods. In [16], although the currents are used as the required signals, its most prominent shortcoming is the lack of robustness against voltage quality problems. In [17], there is an acceptable accuracy in the detection of inter-turn faults. However, it is vulnerable to voltage quality problems. The proposed method has shown the highest accuracy with a time delay of 20 ms. Robustness to voltage quality problems including voltage sag, voltage swell, unbalanced supply voltage, and harmonic contamination in the supply voltage is the other merit of the proposed method.

9 Conclusion

Health monitoring of IMs is very important in industry. This paper focuses on SITF detection in IMs, and addresses the challenges faced by fault detection methods including the needs for high accuracy, reduced time delay and ability to distinguish other conditions from a faulty condition. To this end, a blind source separation technique called principal component analysis (PCA) is presented to extract the faulty components of MCS and MVS from the other components. The standard deviation of one of the decomposed vectors as a statistical SITF criterion is introduced. To improve the robustness of the proposed method against voltage quality problems, three-phase voltage signals are used as auxiliary signals. To verify the reliability of the proposed method, various simulation and practical scenarios are implemented, and the performances are compared with the other MCS-based and MVS-based methods. As an overall trend, the main advantages of the proposed method over other state-of-the-art algorithms include: (a) being the most accurate in diagnosing conditions; (b) capability of detection of faults in 0.02 s; (c) robustness to voltage quality problems; and (d) simplicity in implementation and no need to install additional sensors. It is confirmed that the performance of the proposed criterion is robust to different fault resistances considering different fault intensities. In addition, the proposed criteria can overcome the

voltage quality problems including sag, swell, unbalanced supply voltage, and harmonic contamination in the supply voltage.

The proposed method shows good performance in noisy conditions and during abrupt load change. Consequently, it can be considered as an alternative for the detection of a SITF in IMs.

List of symbols

$[V_{abcs}]$: Three-phase stator voltages; $[I_{abcs}]$: Three-phase stator currents; $[I_{abcr}]$: Three-phase rotor currents; I_f: Stator short-circuit current; λ_f: Stator short-circuit flux; R_s: Stator winding resistance; N_s: The total number turns in each phase; R_r: Rotor winding resistance; R_f: Fault resistance; $[L_{ss}]$: Stator self and mutual inductances matrix; $[L_{rr}]$: Rotor self and mutual inductances matrix; $[L_{sr}]$: Mutual inductances matrix of the stator and rotor phase winding; $[L_{sf}]$: Mutual inductance vector of the stator winding and the faulty turns; $[L_{rf}]$: Mutual inductance vector of rotor winding and the faulty turns; L_{ff}: Self-inductance of the faulted turns; T_{em}: Electromagnetic torque; T_L: Load torque; ω_r: Rotor speed; θ_r: Rotor angle; P: Number of poles; J: Rotor inertia; $[V_{qd0s}]$: Three-phase stator voltages in the qd0 reference frame; $[I_{qd0s}]$: Three-phase stator currents in the qd0 reference frame; $[\lambda_{qd0s}]$: Three-phase stator fluxes in the qd0 reference frame; $[I_{qd0r}]$: Three-phase rotor currents in the qd0 reference frame; $[\lambda_{qdr}]$: Three-phase rotor fluxes in the qd reference frame; L_{ls}: Stator leakage inductance; L_{lr}: Rotor leakage inductance; L_m: Magnetizing inductance.

Abbreviations

IMs: Induction motors; SITF: Stator inter-turn fault; PCA: Principal component analysis; MCS: Motor current signatures; MVS: Motor voltage signatures; FFT: Fast Fourier transform; STFT: Short time Fourier transform; WT: Wavelet transform; PC: Principal components; ITHDs: Instantaneous total harmonic distortions; CT: Current transformer; PT: Potential transformer.

Acknowledgements

The authorsincerely thank to School of Electrical and Computer Engineering, Shiraz University, Shiraz, Iran.

Author contributions

The author read and approved the final manuscript.

Funding

Not applicable.

Availability of data and materials

Not applicable.

Declarations

Competing interests

The authors declare that they have no known competing financial interests or personal relationships that could have appeared to influence the work reported in this paper.

Received: 3 August 2021 Accepted: 16 November 2022
Published online: 01 December 2022

References

1. Abid, F. B., Sallem, M., & Braham, A. (2019). Robust interpretable deep learning for intelligent fault diagnosis of induction motors. *IEEE Trans Instrum Meas, 69*(6), 3506–3515.
2. Hassan, O. E., Amer, M., Abdelsalam, A. K., & Williams, B. W. (2018). Induction motor broken rotor bar fault detection techniques based on fault signature analysis–a review. *IET Electric Power Appl, 12*(7), 895–907.
3. Liang, X., Ali, M. Z., & Zhang, H. (2019). Induction motors fault diagnosis using finite element method: a review. *IEEE Trans Ind Appl, 56*(2), 1205–1217.
4. Maamouri, R., Trabelsi, M., Boussak, M., & M'Sahli, F. (2019). Mixed model-based and signal-based approach for open-switches fault diagnostic in sensorless speed vector controlled induction motor drive using sliding mode observer. *IET Power Electron, 12*(5), 1149–1159.
5. Jiang, S. B., Wong, P. K., Guan, R., Liang, Y., & Li, J. (2019). An efficient fault diagnostic method for three-phase induction motors based on incremental broad learning and non-negative matrix factorization. *IEEE Access, 7*, 17780–17790.
6. Ojaghi, M., Sabouri, M., & Faiz, J. (2014). Diagnosis methods for stator winding faults in three-phase squirrel-cage induction motors. *Int Trans Electr Energy Syst, 24*(6), 891–912.
7. Ghanbari, T. (2016). Autocorrelation function-based technique for stator turn-fault detection of induction motor. *IET Sci Meas Technol, 10*(2), 100–110.
8. Wang, P., Lu, J., Shi, L., Zhang, Y., Tong, Z., & Wang, N. (2020). Method for extracting current envelope for broken rotor bar fault detection of induction motors at time-varying loads. *IET Electr Power Appl, 14*(6), 1067–1077.
9. Panagiotou, P. A., Arvanitakis, I., Lophitis, N., Antonino-Daviu, J. A., & Gyftakis, K. N. (2019). A new approach for broken rotor bar detection in induction motors using frequency extraction in stray flux signals. *IEEE Trans Ind Appl, 55*(4), 3501–3511.
10. Akhil Vinayak, B., Anjali Anand, K., & Jagadanand, G. (2020). Wavelet-based real-time stator fault detection of inverter-fed induction motor. *IET Electr Power Appl, 14*(1), 82–90.
11. Pathak, R. S. (2009). *The wavelet transform* (Vol. 4). Berlin: Springer Science & Business Media.
12. Jia, Z., Liu, Z., Vong, C. M., & Pecht, M. (2019). A rotating machinery fault diagnosis method based on feature learning of thermal images. *IEEE Access, 7*, 12348–12359.
13. Ali, M. Z., Shabbir, M. N. S. K., Liang, X., Zhang, Y., & Hu, T. (2019). Machine learning-based fault diagnosis for single-and multi-faults in induction motors using measured stator currents and vibration signals. *IEEE Trans Ind Appl, 55*(3), 2378–2391.
14. Glowacz, A., Glowacz, W., Glowacz, Z., & Kozik, J. (2018). Early fault diagnosis of bearing and stator faults of the single-phase induction motor using acoustic signals. *Measurement, 113*, 1–9.
15. Zaparoli, I. O., Rabelo Baccarini, L. M., Lamim Filho, P. C. M., & Batista, F. B. (2020). Transient envelope current analysis for inter-turn short-circuit detection in induction motor stator. *J Braz Soc Mech Sci Eng, 42*(2), 1–12.
16. Ghanbari, T., & Samet, H. (2017). A Kalman filter based technique for stator turn-fault detection of the induction motors. *Int J Emerg Electr Power Syst*. https://doi.org/10.1515/ijeeps-2017-0071
17. Sadeghi, R., Samet, H., & Ghanbari, T. (2018). Detection of stator short-circuit faults in induction motors using the concept of instantaneous frequency. *IEEE Trans Ind Inf, 15*(8), 4506–4515.
18. da Silva, A. M., Povinelli, R. J., & Demerdash, N. A. (2013). Rotor bar fault monitoring method based on analysis of air-gap torques of induction motors. *IEEE Trans Ind Inf, 9*(4), 2274–2283.
19. Drif, M. H., & Cardoso, A. J. M. (2014). Stator fault diagnostics in squirrel cage three-phase induction motor drives using the instantaneous active and reactive power signature analyses. *IEEE Trans Ind Inf, 10*(2), 1348–1360.
20. Karmakar, S., Chattopadhyay, S., Mitra, M., & Sengupta, S. (2016). Analytical tools for motor fault diagnosis. In S. Karmakar, S. Chattopadhyay, M. Mitra, & S. Sengupta (Eds.), *Induction motor fault diagnosis* (pp. 29–55). Singapore: Springer Singapore. https://doi.org/10.1007/978-981-10-0624-1_3
21. Duan, F., & Živanović, R. (2014). Condition monitoring of an induction motor stator windings via global optimization based on the hyperbolic cross points. *IEEE Trans Ind Electron, 62*(3), 1826–1834.
22. Chang, H. C., Lin, S. C., Kuo, C. C., & Hsieh, C. F. (2016). Induction motor diagnostic system based on electrical detection method and fuzzy algorithm. *Int J Fuzzy Syst, 18*(5), 732–740.
23. Filippetti F, Martelli M, Franceschini G, Tassoni C. Development of expert system knowledge base to on-line diagnosis of rotor electrical faults of induction motors. In: Conference record of the 1992 IEEE industry applications society annual meeting. IEEE; 1992. pp. 92–99.

24. Bazan, G. H., Scalassara, P. R., Endo, W., Goedtel, A., Godoy, W. F., & Palacios, R. H. C. (2017). Stator fault analysis of three-phase induction motors using information measures and artificial neural networks. *Electric Power Syst Res, 143*, 347–356.
25. Kumar, P., & Hati, A. S. (2021). Review on machine learning algorithm based fault detection in induction motors. *Arch Comput Methods Eng, 28*(3), 1929–1940.
26. Cherif, H., Benakcha, A., Laib, I., Chehaidia, S. E., Menacer, A., Soudan, B., & Olabi, A. G. (2020). Early detection and localization of stator inter-turn faults based on discrete wavelet energy ratio and neural networks in induction motor. *Energy, 212*, 118684.
27. Bensaoucha, S., Brik, Y., Moreau, S., Bessedik, S. A., & Ameur, A. (2021). Induction machine stator short-circuit fault detection using support vector machine. *COMPEL Int J Comput Math Electr Electron Eng*. https://doi.org/10.1108/COMPEL-06-2020-0208
28. Zhou, Z., Wen, C., & Yang, C. (2016). Fault isolation based on k-nearest neighbor rule for industrial processes. *IEEE Trans Ind Electron, 63*(4), 2578–2586.
29. Rafiee, J., Arvani, F., Harifi, A., & Sadeghi, M. H. (2007). Intelligent condition monitoring of a gearbox using artificial neural network. *Mech Syst Signal Process, 21*(4), 1746–1754.
30. Saravanan, N., & Ramachandran, K. I. (2009). Fault diagnosis of spur bevel gear box using discrete wavelet features and decision tree classification. *Expert Syst Appl, 36*(5), 9564–9573.
31. Palacios, R. H. C., Da Silva, I. N., Goedtel, A., & Godoy, W. F. (2015). A comprehensive evaluation of intelligent classifiers for fault identification in three-phase induction motors. *Electr Power Syst Res, 127*, 249–258.
32. Kumar, P., & Shankar Hati, A. (2021). Convolutional neural network with batch normalisation for fault detection in squirrel cage induction motor. *IET Electr Power Appl, 15*(1), 39–50.
33. Liu, H., Zhou, J., Zheng, Y., Jiang, W., & Zhang, Y. (2018). Fault diagnosis of rolling bearings with recurrent neural network-based autoencoders. *ISA Trans, 77*, 167–178.
34. Wang, B., Shen, C., Xu, K., & Zheng, T. (2019). Turn-to-turn short circuit of motor stator fault diagnosis in continuous state based on deep auto-encoder. *IET Electr Power Appl, 13*(10), 1598–1606.
35. Jalayer, M., Orsenigo, C., & Vercellis, C. (2021). Fault detection and diagnosis for rotating machinery: a model based on convolutional LSTM, Fast Fourier and continuous wavelet transforms. *Comput Ind, 125*, 103378.
36. De La Barrera, P. M., Bossio, G. R., Solsona, J. A., & Garcıa, G. O. (2010). Model for three-phase induction motors with stator core faults. *IET Electr Power Appl, 4*(8), 591–602.
37. Patel, D. C., & Chandorkar, M. C. (2013). Modeling and analysis of stator interturn fault location effects on induction machines. *IEEE Trans Ind Electron, 61*(9), 4552–4564.
38. Armah KE, Jouffroy J, Duggen L. Modeling induction motor imbalances: a non-DQ approach. In: 2016 IEEE international conference on advanced intelligent mechatronics (AIM). IEEE; 2016. pp. 769–774.
39. Ojaghi, M., Sabouri, M., & Faiz, J. (2018). Performance analysis of squirrel-cage induction motors under broken rotor bar and stator inter-turn fault conditions using analytical modeling. *IEEE Trans Magn, 54*(11), 1–5.
40. Otsu, N. (1979). A threshold selection method from gray-level histograms. *IEEE Trans Syst Man Cybern, 9*(1), 62–66.
41. Arrillaga, J., Arrillaga, J., Watson, N. R., Watson, N. R., & Chen, S. (2000). *Power system quality assessment*. New York: Wiley-Blackwell.
42. Ostojic P, Banerjee A, Patl D, Basu W, Ali S. Advanced motor monitoring and diagnostics. In: Industry applications society 60th annual petroleum and chemical industry conference. IEEE; 2013. pp. 1–9.